

1 **Efficient CRISPR genome editing and integrative genomic analyses reveal the mosaicism of**  
2 **Cas-induced mutations and pleiotropic effects of *scarlet* gene in an emerging model system**

3 Sen Xu<sup>1\*</sup>, Swatantra Neupane<sup>1§</sup>, Hongjun Wang<sup>2§†</sup>, Thinh Phu Pham<sup>2§</sup>, Marelize Snyman<sup>2¶</sup>,  
4 Trung V. Huynh<sup>1</sup>, Li Wang<sup>1</sup>

5 <sup>1</sup>Division of Biological Sciences, University of Missouri, Columbia, Missouri, 65211, USA

6 <sup>2</sup>Department of Biology, University of Texas at Arlington, Arlington, Texas, 76019, USA

7 <sup>†</sup>Current address: Department of Neurology, University of Texas Southwestern Medical Center,  
8 Dallas, TX 75235, USA

9 <sup>¶</sup>Current address: Department of Dermatology, University of Texas Southwestern Medical  
10 Center, Dallas, TX 75235, USA

11

12 <sup>§</sup>Equally contributing authors.

13

14 \*Corresponding author. Email: [sxwf7@umsystem.edu](mailto:sxwf7@umsystem.edu)

15

16 **Running title:** CRISPR genomic editing in *Daphnia pulex*

17 **Keywords:** mutation, Cas, knock-in, swimming behavior, off-target mutation

## 18 **Abstract**

19 Despite the revolutionary impacts of CRISPR-Cas gene editing systems, the effective and  
20 widespread use of CRISPR technologies in emerging model organisms still faces significant  
21 challenges. These include the inefficiency in generating heritable mutations at the organismal  
22 level, limited knowledge about the genomic consequences of gene editing, and an inadequate  
23 understanding of the inheritance patterns of CRISPR-Cas-induced mutations. This study  
24 addresses these issues by 1) developing an efficient microinjection delivery method for CRISPR  
25 editing in the microcrustacean *Daphnia pulex*; 2) assessing the editing efficiency of Cas9 and  
26 Cas12a nucleases, examining mutation inheritance patterns, and analyzing the local and global  
27 mutation spectrum in the *scarlet* mutants; and 3) investigating the transcriptomes of *scarlet*  
28 mutants to understand the pleiotropic effects of *scarlet* underlying their swimming behavior  
29 changes. Our reengineered CRISPR microinjection method results in efficient biallelic editing  
30 with both nucleases. While indels are dominant in Cas-induced mutations, a few on-site large  
31 deletions (>1kb) are observed, most likely caused by microhomology-mediated end joining  
32 repair. Knock-in of a stop codon cassette to the *scarlet* locus was successful, despite complex  
33 induced mutations surrounding the target site. Moreover, extensive germline mosaicism exists in  
34 some mutants, which unexpectedly produce different phenotypes/genotypes in their asexual  
35 progenies. Lastly, our transcriptomic analyses unveil significant gene expression changes  
36 associated with *scarlet* knock-out and altered swimming behavior in mutants, including several  
37 genes (e.g., NMDA1, ABAT, CNTNAP2) involved in human neurodegenerative diseases. This  
38 study expands our understanding of the dynamics of gene editing in the tractable model organism  
39 *Daphnia* and highlights its promising potential as a neurological disease model.

40

## 41 **Introduction**

42 CRISPR-mediated gene editing systems (Jinek et al. 2012; Cong et al. 2013; Mali et al. 2013)  
43 have become a primary tool for introducing DNA sequence modifications in target nuclear  
44 genomic regions because of their simplicity and ease of use. When fused with a guide RNA  
45 (gRNA), CRISPR nucleases can cause DNA double-strand breaks (DSBs) at a target sequence  
46 location that is complementary to the gRNA sequence. Without a DNA repair template, the  
47 DSBs can be repaired by the error-prone non-homologous end joining (NHEJ) pathway,  
48 resulting in indels and disruption of gene function (Hefferin and Tomkinson 2005; Rodgers and  
49 McVey 2016). When a homologous DNA template is provided, DSBs can be repaired through  
50 homology-directed recombination (HDR) by template-directed DNA synthesis to bridge the gap  
51 across DSBs (Liang et al. 1998; Sekelsky 2017). These features of the CRISPR editing system  
52 thus offer flexible control of the genomic locations and outcomes of the genetic modifications.

53 More importantly, CRISPR-Cas technologies (Jinek et al. 2012; Cong et al. 2013; Mali  
54 et al. 2013) have democratized the genetic and genomic research landscape, providing an  
55 important means of genetic engineering to emerging model systems that traditionally lack tools  
56 for genetic manipulation. The past few years have witnessed the successful implementation of  
57 CRISPR-mediated gene editing in organisms such as squids (Crawford et al. 2020), raider ants  
58 (Trible et al. 2017), black-legged tick (Sharma et al. 2022), cockroaches (Shirai et al. 2022) and  
59 lizards (Rasys et al. 2019), to name a few. Nonetheless, efficiently generating heritable biallelic  
60 mutations remains one of the most significant challenges involved in implementing CRISPR-  
61 Cas9 gene editing in emerging model systems.

62 In this study, we present a highly efficient microinjection-based method for generating  
63 heritable, biallelic knock-out mutations and evaluate the efficiency for knock-in mutations using

64 the CRISPR-Cas system in the freshwater microcrustacean *Daphnia pulex*. *Daphnia* has been a  
65 model system for ecology, evolution, and toxicology for several decades (Miner et al. 2012;  
66 Ebert 2022). As the first whole-genome sequenced crustacean species (Colbourne et al. 2011), *D.*  
67 *pulex* has become an important genomics model system for gene-environment interaction  
68 (Altshuler et al. 2011), epigenetics (Harris et al. 2012), and evolutionary genomics (Lynch et al  
69 2017). There is also growing interest in using *Daphnia* as a model in studying the evolution of  
70 development because *Daphnia* represents an important phylogenetic lineage in invertebrate  
71 evolution (Rivera et al. 2010; Mahato et al. 2014; Bruce and Patel 2022). Therefore, an efficient  
72 gene editing method would be invaluable for the genetic toolkit of *Daphnia* to unleash its full  
73 potential as an emerging model system.

74 Microinjection into embryos has been a major means of genetic manipulation in  
75 *Daphnia*. Under benign environmental conditions female *Daphnia* reproduce asexually through  
76 the production of ameiotic diploid embryos that directly develop into neonates in 2-3 days,  
77 whereas in stressful environments female *Daphnia* produces haploid eggs and mate with males  
78 to produce diploid dormant embryos (**Figure 1**). The asexual reproductive stage provides an  
79 excellent platform for microinjection-based genomic engineering. Many asexual embryos can be  
80 easily collected for injection from females of the same genotype. After microinjection, the  
81 injected embryos can quickly hatch into neonates ( $G_0$  generation) in 2-3 days, and  $G_0$  individuals  
82 can have asexual progenies ( $G_1$  generation) in ~7 days, which guarantees a fast turn-around time  
83 for phenotypically and genotypically identifying  $G_0$  and  $G_1$  mutants. Furthermore, the asexual  
84 reproduction mode allows the long-term preservation of stable mutant genotypes with low  
85 maintenance efforts.

86 Building on these advantages, microinjection techniques have been developed for  
87 *Daphnia* to deliver biomolecules into the asexually produced embryos to achieve gene  
88 knockdown through RNAi (Kato et al. 2011; Hiruta et al. 2013), protein tagging (Kato et al.  
89 2012), gene knock-out using CRISPR-Cas9 (Ismail et al. 2018), and knock-in using TALEN  
90 (Nakanishi et al. 2016). The successful development of these techniques has empowered  
91 important discoveries at the molecular level such as the molecular mechanisms of environmental  
92 sex determination in *Daphnia magna* (Kato et al. 2018).

93 However, it should be noted that most of these previous efforts focused on the species  
94 *Daphnia magna*, a species has diverged ~200-million years ago from the focal species of this  
95 study *D. pulex* (Colbourne and Hebert 1996). *D. magna* has a substantially larger body size and  
96 larger embryo size compared to *D. pulex* (Toyota et al. 2016). Modified microinjection protocols  
97 have therefore been developed for *D. pulex* to deal with the technical challenges associated with  
98 these variations, for example, internal osmotic pressure in the embryos (Hiruta et al. 2013).  
99 However, no efforts have aimed at establishing a microinjection procedure for creating heritable  
100 biallelic knock-out and knock-in genotypes using CRISPR-Cas in *D. pulex*. Although knocking  
101 out the Hox gene *distalless* was successful in *D. pulex* using CRISPR-Cas9 (Hiruta et al. 2018),  
102 no biallelic knock-out lines were created because complete knockout of *distalless* is lethal.

103 More importantly, given that CRISPR-Cas system can cause spurious off-target  
104 mutations or on-target complex mutations in various model systems (Fu et al. 2013; Aryal et al.  
105 2018; Höijer et al. 2022), it is imperative to systematically evaluate the mutations induced by  
106 CRISPR-Cas in the *Daphnia* system. However, such studies are still lacking to date.

107 To create heritable biallelic mutations in an efficient manner, it is critical to accurately  
108 deliver RNPs (ribonucleotide proteins - Cas9 fused with gRNAs) or plasmids into the nucleus of

109 an embryo at the one-cell stage. In the hope of accomplishing this at a high efficiency, we first  
110 consider the timing of key events in the development of asexually produced embryos in *D. pulex*.  
111 During the asexual reproduction in female *Daphnia*, oocytes go through a modified meiosis (i.e.,  
112 ameiosis) to produce chromosomally unreduced diploid embryos. In ameiosis, the original  
113 meiosis I is modified, resulting in suppressed recombination and no cytokinesis, while meiosis II  
114 remains normal and produces a polar body and a diploid embryo in the end (Hiruta et al. 2010).  
115 These asexually produced embryos can directly develop into neonates in the female's brood  
116 chamber without fertilization.

117 The cytology of ameiosis in *Daphnia* has been carefully examined (Ojima 1958;  
118 Zaffagnini and Sabelli 1972; Hiruta et al. 2010). The ameiotic division begins with the  
119 breakdown of germinal vesicle while the eggs are still in the ovary of females, which also  
120 coincides with the timing of female molting. Ovulation (i.e., embryos moving into brood  
121 chamber from ovary) begins approximately 10-15 minutes after molting. Upon entering the  
122 brood chamber, the egg cell enters anaphase I, with chromosomes staying near the periphery of  
123 embryo (Ojima 1958; Zaffagnini and Sabelli 1972). The ameiotic division proceeds to anaphase  
124 II in approximately 10 minutes post ovulation and the entire division process is completed 20  
125 minutes post-ovulation with polar body emission (Hiruta et al. 2010). At this point the  
126 chromosomes move to the deeper part of the embryo, the nucleus membrane re-emerges, and the  
127 first cleavage division is finished around 20-60 minutes post-ovulation (Ojima 1958; Hiruta et al.  
128 2010).

129 Considering this timeline of key events, we suggest that the first 10 minutes post-  
130 ovulation (approximately between anaphase I to anaphase II) provides an optimal time window  
131 for microinjecting RNPs for introducing biallelic heritable modifications. The oocyte remains in

132 the one-cell stage at this interval, during which the delivered RNPs would have opportunities to  
133 bind to chromosomes once the target loci become accessible (e.g., chromosomes exist in a less  
134 condensed state) during or after the ameiotic division. Also, microinjecting at an early timepoint  
135 is critical for the successful hatching of injected embryos because *Daphnia* embryos rapidly lose  
136 their membrane elasticity once ovulated and only early embryos with elastic membranes can  
137 sustain the damages caused by microinjection (Kato et al. 2011).

138 In addition to knowing when to deliver the RNPs alone into the embryo, understanding  
139 where in the embryo to deliver the RNPs is also critical for successful gene editing. The small  
140 size of the asexual embryos (with a diameter ~50-100  $\mu\text{m}$ ) in *D. pulex* and the presence of  
141 massive amount of egg yolk and fat droplets in the embryos make it infeasible to locate the  
142 whereabouts of the nucleus or chromosomes during oogenesis under a typical stereomicroscope  
143 used for microinjection. Considering that the chromosomes undergo movement from a peripheral  
144 spot near the embryo membrane to a more central part of the embryo after the ameiotic division  
145 (Ojima 1958; Hiruta et al. 2010), an effective microinjection strategy would be to deliver a  
146 concentrated dose of RNPs close to the center of the embryo so that the RNPs can rapidly spread  
147 within the embryo to maximize possibilities of binding the targeted chromosomal loci.

148 Incorporating these considerations, we have developed a set of optimal practices for  
149 microinjection experiments for CRISPR-Cas genomic editing in *D. pulex* (**Figure 2**). In this  
150 study, we test the efficiency of Cas9 and Cas12a nucleases for generating a heritable biallelic  
151 *scarlet* gene knock-out. Also, we use Cas9 to create knock-in alleles at the *scarlet* gene. The  
152 SCARLET protein is responsible for transporting tryptophan, precursors of eye pigment (Ewart  
153 et al. 1994). Therefore, disruption of the *scarlet* gene can result in clear-eyed mutant daphniids  
154 that can be readily distinguished from the wild-type black-eyed individuals (Ismail et al. 2018).

155 We also introduce a few other innovative modifications (e.g., microinjection needles, injection  
156 stage) to the existing microinjection system of *Daphnia* to substantially increase its efficiency.

157 Furthermore, we analyzed the whole-genome DNA sequences of the knock-out and  
158 knock-in mutants to assess the potential of off-target modifications and on-target mutation  
159 accuracy in the *D. pulex* genome. Lastly, because knocking out ABC transporters including the  
160 *scarlet* gene and *white* gene have pleiotropic impacts on the levels of biogenic amines in the  
161 brain (Borycz et al. 2008), male courtship behavior (Anaka et al. 2008), and cyclic GMP  
162 transportation (Evans et al. 2008), we examined the altered swimming behavior of *scarlet*  
163 mutants and performed RNA-seq experiments to investigate its possible causes and to understand  
164 the pleiotropic effects of the *scarlet* gene on genome-wide transcriptomic abundance.

## 165 **Materials and Methods**

### 166 *Experimental animals*

167 We maintained a healthy culture of 2-3-week-old *Daphnia* females that were all asexually  
168 derived from a single, natural *Daphnia* isolate EB1 (Eloise Butler, Minnesota). We kept these  
169 animals in artificial lake water COMBO (Kilham et al., 1998) at 25 °C and under a 16:8  
170 (light:dark hours) photoperiod. Because we needed asexually reproducing females for collecting  
171 asexual embryos, the animals were fed with the green algae *Scenedesmus obliquus* every day and  
172 the newly born babies were removed every other day to prevent overcrowding that can trigger  
173 *Daphnia* to switch to sexual reproduction.

### 174 *Microinjection equipment*

175 We used Eppendorf FemtoJet 4i microinjector and Injectman 4 micromanipulator to perform  
176 microinjection on *Daphnia* embryos under a Nikon SMZ800N dissection microscope. We

177 prepared microinjection needles using aluminosilicate glass capillaries (catalog no. AF100-64-  
178 10, Sutter Instrument). We chose the aluminosilicate glass rather than regular borosilicate glass  
179 because it penetrates the chorion and membrane of *Daphnia* embryos at high efficiency and  
180 incurs little clogging at a fine tip size. Microinjection needles were pulled to have a final  
181 specification of ~1.5- $\mu$ m tip size and ~7-mm taper length on a P-1000 needle puller (Sutter  
182 Instrument), using the following pulling parameters: heat 535 (ramp test value 525 + 10), pull  
183 65, velocity 70, time 200, and pressure 250. The pulled needles were beveled on a BV-10  
184 micropipette beveler (Sutter instrument) with a fine 104D grinding plate (Sutter Instrument)  
185 covered by a thin layer of soap water to forge a 30-degree bevel at the tip. The beveled needles  
186 were then immediately cleaned using 100% ethanol to remove contaminating debris introduced  
187 during pulling and beveling.

#### 188 *CRISPR-Cas reagents*

189 For the knock-out experiments at the *scarlet* locus using Cas9, we designed one crRNA  
190 (**Supplementary Table S1**) targeting the exon 1 and one crRNA for exon 2 using the Design  
191 Custom gRNA tool from IDT (Integrated DNA Technologies) based on the DNA sequence of  
192 the EB1 isolate (**Figure 2B**). These sgRNAs were chemically synthesized (Alt-R<sup>TM</sup> custom  
193 sgRNAs, IDT). To prepare the RNPs, equal molar amount of each sgRNA and the tracrRNA  
194 (Alt-R<sup>TM</sup> crRNA, IDT) was mixed and incubated at 95 °C for 5 min and cooled to room  
195 temperature to form the guide RNA. The guide RNA was subsequently mixed with Cas9 enzyme  
196 (catalog no. 1081058, IDT) and was incubated at room temperature for 15 minutes. We co-  
197 injected two different RNPs into embryos, with each sgRNA at a concentration of 125 ng/ $\mu$ l and  
198 Cas9 enzyme at 600 ng/ $\mu$ l.

199 For knocking out *scarlet* using Cas12a nuclease (Cpf1), we designed one crRNA  
200 targeting a 21-nucleotide sequence for the exon 1 and exon 2 each (**Figure 2B, Supplementary**  
201 **Table S1**). To prepare RNP, the Alt-R™ A.s. Cas12a nuclease V3 (catalog no. 1081068, IDT)  
202 was fused with crRNA at equal molar amounts at room temperature. We co-injected two  
203 different RNPs into embryos, with each sgRNA at a concentration of 125 ng/μl and Cas12a  
204 nuclease at 600 ng/μl.

205 For the knock-in experiment at the *scarlet* locus using Cas9 nuclease, we designed a  
206 HDR template for repairing the double-strand break at the crRNA2 target site (**Supplementary**  
207 **Table S1**). This HDR template was chemically synthesized ssDNA (IDT), containing a stop  
208 codon cassette flanked by homology arms of 40 bp on each end. If successfully inserted at the  
209 target locus, it would disrupt the translation of the scarlet gene because the stop codon cassette  
210 presents stop codons in all the six possible reading frames.

#### 211 *Embryo collection for microinjection experiments*

212 For each microinjection experiment, we screened our animal culture to select a large number  
213 (~100-150) of females that showed inflated dark ovary, indicating they would likely molt and  
214 ovulate in a few hours. Each of the selected animals was placed in a drop of COMBO artificial  
215 lake water containing 60 mM sucrose. These animals were regularly checked for signs of  
216 molting. The molted animals were closely monitored for signs of ovulation (i.e., oocytes starting  
217 to enter the brood chamber), which usually occurs 10-15 minutes after molting (**Figure 2**). Once  
218 a female started ovulation and ~80% of embryos entered the brood chamber (**Figure 2**), we  
219 transferred this female to an ice-cold (~1.5 °C) solution of COMBO with 60 mM sucrose.

220 We let the female stay in the ice-cold solution for approximately 5 minutes and then  
221 dissected the embryos out. We chose the 5-minute wait time because the oocytes should still be  
222 undergoing ameiotic division (see Introduction) while the cold temperature slows down the  
223 activities of cellular machinery.

224 The dissection was performed on the bottom surface of a small petri dish flipped upside  
225 down (60 mm x 15 mm, catalog no. FB0875713A, Fisher Scientific). After we removed the body  
226 of the daphniid, we aligned the embryos against the slightly raised edge of the petri dish. We also  
227 removed the excessive solution surrounding the embryos, leaving the embryos submerged under  
228 a thin layer of solution.

#### 229 *Microinjection*

230 We backloaded a microinjection needle with 1  $\mu$ l of RNP using a microloader tip (Eppendorf, cat  
231 no. 930001007). We aimed to inject 1-2 nl of RNP into the embryo. With each needle being  
232 different, the injection pressure was generally between 100 and 220 hPa, whereas the  
233 background pressure was between 100 and 200 hPa, with an injection time of 0.8 second.

234 Once the embryos were ready for injection, we immediately performed the injection  
235 procedure (**Figure 2**). We injected the RNPs near the center of the embryo. Once the injection  
236 was completed, we added COMBO with 60 mM sucrose to the embryos and left the embryos in  
237 this condition for ~30 minutes at room temperature (Cas9) or for 2 hours at 33°C (Cas12a). Then  
238 we transferred the injected embryos to a 24-well plate containing COMBO artificial lake water  
239 and cultured the embryos at 25°C. Embryos usually hatched into neonates in ~48 hours at this  
240 temperature.

#### 241 *Mutant screening*

242 Among the hatched neonates from the injected embryos ( $G_0$  individuals), we searched for  
243 individuals with a clear eye or an eye of partially missing black pigment (i.e., mosaic  
244 individuals) as tentative knock-out and knock-in mutants. We kept these  $G_0$  neonates and  
245 examined their progenies. If all the asexually produced  $G_1$  offspring of a  $G_0$  mutant were clear-  
246 eyed, we concluded that the  $G_0$  individual carried biallelic knock-out mutations at the scarlet  
247 locus. We established a clonal mutant line using the  $G_0$  individual and its asexual progenies.

248 For the mosaic individuals, we examined the eye phenotype in the different broods of  $G_0$   
249 individuals. We recorded the number of clear-eye and black-eye individuals and established  
250 mutant lines using a single clear-eye individual from the same or different broods.

#### 251 *Whole-genome sequencing and mutation identification*

252 To investigate whether off-target mutations occur in the knock-out and knock-in mutants, we  
253 performed whole-genome sequencing on the asexually produced offspring of each established  
254 mutant line plus the wildtype. DNA of mutant lines was extracted from pooled samples of 3<sup>rd</sup>  
255 and 4<sup>th</sup> generation offspring using a CTAB protocol (Wang and Xu 2021). The DNA sequencing  
256 library was prepared by BGI America or by us, and the genome sequencing was performed on a  
257 DNB sequencing or Illumina NovaSeq 6000 platform with 150-bp paired-end reads. Each mutant  
258 line was sequenced at ~30x coverage per nucleotide site. Raw reads are available at NCBI SRA  
259 (Sequence Read Archive) under project PRJNA1055485.

260 We aligned the raw reads of each mutant/wildtype line to the *D. pulex* PA42 reference  
261 assembly 3.0 (Ye et al. 2017) using the Burrows-Wheeler Alignment Tool BWA-MEM version  
262 0.7.17 (Li and Durbin 2010). We removed reads mapped to multiple locations in the genome and  
263 retained only uniquely mapped reads for identifying mutations. We generated calls of single

264 nucleotide variants and indels using the mpileup and call functions of BCFtools (Danecek et al.  
265 2021) for all mutant lines in a single VCF file. Default parameters were used for BCFtools  
266 mpileup and call functions, with the addition of the following FORMAT and INFO tags to the  
267 VCF file: AD (allelic depth), DP (number of high-quality bases), ADF (allelic depth on forward  
268 strand) and ADR (allelic depth on reverse strand). We retained only biallelic single nucleotide  
269 polymorphism sites (SNPs) with a quality score (QUAL)  $\geq 20$ , sequencing depth (DP)  $\geq 10$ ,  
270 and a distance  $\geq 50$  bp from an indel in each mutant line.

271 A custom Python script was used to identify mutations in each mutant line using a  
272 consensus method. For each SNP site, we established the consensus wildtype genotype call using  
273 a majority rule: with a total of N samples in a VCF file, the consensus genotype of a site needs to  
274 be supported by at least N-1 samples. If a mutant line shows a genotype different from the  
275 consensus genotype, a tentative mutation is identified.

276 These tentative mutations must meet two criteria to enter the final pool of mutations.  
277 First, a mutant allele had to be supported by at least two forward and two reverse reads to avoid  
278 false positives due to sequencing errors. Second, a mutant genotype was recognized only when it  
279 is a heterozygous genotype derived from a homozygous wildtype genotype. This criterion is to  
280 avoid false positives caused by allele dropout due to insufficient sequence coverage or artifacts  
281 in library construction at heterozygous sites. This computation pipeline was experimentally  
282 verified in a previous study with a false positive rate  $< 0.05$  (Snyman et al. 2021).

283 Furthermore, we examined whether any of the identified mutations in the mutant lines  
284 occur within a 100-bp vicinity of any nucleotide sequence that is a blast hit with E value  $> 0.01$   
285 to the gRNA target sequences.

286 *Structural variation detection*

287 To understand whether the mutants harbored any off-target structural variations caused by Cas  
288 nucleases, we used the SV caller Manta (Chen et al. 2016) to identify SVs in all the *scarlet*  
289 mutants. Due to the limited power of short-read data in detecting SVs such as inversions, we  
290 restricted our analysis to large indels and duplications. In addition to the mutants, we performed  
291 genomic sequencing on the wildtype strain. To identify newly arising SVs in the wildtype  
292 genomic background, we performed paired analysis between the wildtype and each mutant,  
293 where the wildtype served as the control and the mutant represented treatment. All the SV calls  
294 excluded imprecise predictions and any variants with a score below 30, thereby mitigating the  
295 risk of false positives.

296 *Behavioral and life-history assay of scarlet mutants*

297 We examined whether the scarlet mutant females (KO2 and KO3) display excessive spinning  
298 swimming behavior compared to the wildtype, as reported in the *scarlet* mutant of another  
299 *Daphnia* species *D. magna* (Ismail et al. 2021). As we found the wildtype females frequently  
300 spins when they try to release babies from their brood pouch, we examined mutant and wildtype  
301 females that were 1-day old to 5-day old to avoid this confounding effect. Animals were placed  
302 in a 20ml scintillation vial with COMBO artificial lake water under an LED light. We started  
303 observing them after 30 minutes of acclimation. We counted the number of spins per minute  
304 within a 1-hour window.

305 *RNA-seq data collection*

306 Transcriptomic sequencing was performed with 2- or 3-day old neonates of seven scarlet mutant  
307 lines (KO1, KO2, K03, K04, KI2, KI3, and KI4) and the wildtype to understand how the scarlet

308 knock-out genotype reshaped genome-wide transcript abundance. Three replicate RNA-seq  
309 libraries were sequenced for each sample on an Illumina NovaSeq 6000 platform with 150-bp  
310 paired-end reads. The raw RNA sequencing data for this project can be found at NCBI SRA  
311 under PRJNA1060702. Additional notes about details of our RNA-seq experiments and analyses  
312 are available in the Supplementary Materials.

### 313 *Differential expression analysis*

314 We examined the raw read quality using FastQC  
315 (<https://www.bioinformatics.babraham.ac.uk/projects/fastqc/>). Adapter trimming and quality  
316 filtering were completed using Trimmomatic v.0.39 (Bolger et al. 2014). Trimmed reads were  
317 mapped to the *Daphnia pulex* reference genome PA42 3.0 (Ye et al. 2017) using STAR aligner  
318 (Dobin et al. 2013) with default parameters. Reads mapping to multiple locations were removed  
319 using SAMtools (Li et al. 2009), and the program featureCounts (Liao et al. 2014) was used to  
320 obtain the raw read counts for each sample. Differential expression analysis was performed using  
321 DESeq2 v.1.34.0 (Love et al. 2014) using the Wald negative binomial test. To obtain an  
322 overview of the transcriptomic differences between all *scarlet* mutants and the wildtype, we  
323 pooled and compared all mutants against the control samples. Also, we compared the  
324 transcriptome of each mutant line with that of the wildtype for differential expression. We  
325 adjusted p-values for multiple testing using the Benjamini-Hochberg method as implemented in  
326 DESeq2. Genes were considered differentially expressed if they had an adjusted p-value of <  
327 0.05 and greater than a 1.5-fold change. Our scripts are available at  
328 <https://github.com/Marelize007/Scarlet>.

### 329 *Co-expression analysis*

330 To identify co-expressed gene modules and to explore the association between gene networks  
331 and the scarlet phenotype, we performed Weighted Gene Co-expression Network Analysis  
332 (WGCNA, Langfelder and Horvath 2008) to generate a signed co-expression network using the  
333 variance-stabilized read counts for the scarlet mutants and wild-type. For computational  
334 efficiency, we restricted the analysis to the top 50% of the most variable genes (n=7093).  
335 Clusters of highly co-expressed genes were identified by constructing the topological overlap  
336 matrices, a measure of interconnection between genes, with a soft cut-off threshold of 14 using  
337 the blockwiseModule function (see Supplementary Materials for additional technical details).

338 Module eigengenes were calculated using the moduleEigengene function. Module  
339 eigengenes can be defined as the most representative gene within a module and allow us to study  
340 how related the modules are and the correlation between modules and phenotypic traits. An  
341 eigengene heatmap (**Supplementary Figure S1**) was constructed to visualize the correlation  
342 between modules and the *scarlet* knock-out phenotype.

343 Lastly, we constructed a network of differentially expressed genes in the red module to  
344 visualize the correlations between them (**Supplementary Figure S2**). Negative correlation  
345 edges were colored black and positive correlation edges were colored red. Only edges with a  
346 Pearson correlation coefficient greater than 0.9 were kept. The size of the vertices was scaled in  
347 proportion to the level of expression of each gene. The genes were further clustered into  
348 communities based on edge betweenness.

349 *Functional enrichment analysis of differentially expressed genes*

350 We performed GO term enrichment analysis using the R package topGO (Alexa and  
351 Rahnenfuhrer 2019) to investigate the biological relevance of differentially expressed genes. The  
352 default algorithm, weight01, was used along with the Fisher's exact test.

353 Furthermore, to detect KEGG pathways enriched for differentially expressed genes, the  
354 GHOSTX program (Moriya et al. 2007) was used to query all the annotated (18,440) genes from  
355 the *D. pulex* PA42 transcriptome (Ye et al. 2017) in the KEGG Automatic Annotation Server  
356 (KAAS). A total of 10,135 genes were assigned a KO (KEGG ortholog) number, of which 6,282  
357 were mapped to KEGG pathways. Enriched pathways were identified through hypergeometric  
358 tests with Holm-Bonferroni correction in a custom script  
359 (<https://github.com/Marelize007/Scarlet>). KEGG pathways with a p-value < 0.05 were  
360 considered significantly enriched with differentially expressed genes.

## 361 **Results**

### 362 *Optimized microinjection methods*

363 Our microinjection method featured a few notable improvements, empowering fast and efficient  
364 microinjection with *Daphnia*. Our needle pulling and beveling procedure consistently generated  
365 injection needles with a tip size of 1-2  $\mu\text{m}$  and 5-6 mm taper. At such fine tip size, the beveled  
366 needle had substantially fewer clogging issues than non-beveled ones, whereas aluminosilicate-  
367 glass needles allowed easier penetration into the embryos than borosilicate-glass needles.  
368 Moreover, dissecting and injecting embryos on the same petri dish stage produced an increased  
369 number of intact embryos for injection, compared to a procedure involving transferring the  
370 newly ovulated embryos (extremely fragile with an irregular shape) from a dissection stage to the  
371 injection stage (which would inevitably damage some embryos). To clearly demonstrate our  
372 microinjection procedure, a video is available through this link (<https://youtu.be/z1Dc0vTAj8A>).

373 *Knock-out and knock-in efficiency at the scarlet locus*

374 Using our optimized microinjection procedure, we were able to consistently perform successful  
375 microinjection of Cas9/Cas12a RNPs into the asexual embryos of *Daphnia* and achieve a  
376 hatching rate of 24-59% for the injected embryos (**Table 1 and Table 2**). In *scarlet* CRISPR-  
377 Cas9 knock-out experiments, the success rates for generating the clear-eye phenotype in G<sub>0</sub>  
378 individuals (**Figure 2C**) ranged from 1% to 15.6% with a median of 3.85%, whereas in the  
379 knock-in experiments the clear-eye phenotype rate was between 1.1% and 3.4% (**Table 1**).  
380 Moreover, we identified mosaic mutants among G<sub>0</sub>s that have reduced black pigments in the  
381 eyes (**Table 1**). For the Cas12a knock-out experiments, the success rates for generating clear-  
382 eyed G<sub>0</sub> individuals were between 0 and 16%, whereas the rate for mosaic individuals ranged  
383 between 0 and 19%.

384 From our knock-in experiments, two out of eight clear-eyed G<sub>0</sub>s were found to have  
385 successful insertion of the stop codon cassette at the scarlet locus. However, the insertion of the  
386 stop codon was accompanied by complex modifications at the target site (see below).

387 *Transmission pattern of scarlet knock-out genotypes*

388 For all the established clear-eyed and mosaic G<sub>0</sub> individuals, we examined the eye phenotype of  
389 their asexual offspring from different broods (G<sub>1</sub> individuals). For all the clear-eyed G<sub>0</sub>s from  
390 Cas9 knock-out/knock-in experiments, all the G<sub>1</sub>s from at least three different broods showed the  
391 clear-eye phenotype, indicating heritable biallelic modifications at the scarlet locus. Moreover,  
392 we examined the asexual G<sub>2</sub> offspring from a random set of clear-eyed G<sub>1</sub>s, and all the G<sub>2</sub>s  
393 showed the same phenotype as their mothers, as expected under asexual reproduction.

394 For the Cas9-produced mutants, we occasionally found a mosaic individual produced  
395 only black-eyed offspring, indicating somatic mutation at the *scarlet* locus. Nonetheless, most

396 mosaic individuals produced clear-eyed offspring, sometimes along with black-eyed siblings. We  
397 noted that no offspring from mosaic individuals exhibited the mosaic phenotype. Some mosaic  
398 individuals produced only clear-eyed offspring, while others interestingly produced both clear-  
399 eyed and black-eyed offspring in the same or different broods (**Figure 3 and Supplementary**  
400 **Table S2**). This observation led us to hypothesize that the asexual offspring of *Daphnia*  
401 originated from different oogonia, some of which were genetically modified by CRISPR-Cas9  
402 and others were not. This also raised the possibility that the genetically modified oogonia may  
403 carry different genetic modifications at the scarlet locus, i.e., mosaicism in the germline cells.

404 On the other hand, we saw an increase of mosaic  $G_0$  individuals (5 out of 8) from Cas12a  
405 knock-out experiments. These mosaic individuals produced only black-eyed  $G_1$ s in all the  
406 examined broods during their life span (**Table S3**). This observation suggests increased somatic  
407 knock-out of *scarlet* with Cas12a nuclease under our experimental conditions. However,  
408 germline knock-out did occur in Cas12a experiments. Some mosaic  $G_0$  individuals and a clear-  
409 eyed individual produced mixed broods (**Figure 3 and Supplementary Table S3**), strongly  
410 indicating germline mosaicism in the  $G_0$ s.

#### 411 *Knock-out genotypes induced by Cas9 nuclease*

412 We used the whole-genome short-read sequences of the mutants to analyze the Cas9-induced  
413 mutations at the *scarlet* locus. In our analyses we were able to phase the two haplotypes of the  
414 scarlet locus and identify the haplotype-specific mutations. Detailed mutation sequence  
415 alignment is available in **Supplementary File 1**. Our analyses showed that, although RNPs  
416 targeting two different sites of the *scarlet* locus were co-injected, only one knock-out mutant  
417 (KO4) contained a homozygous segmental deletion (234 bp) spanning the two target sites  
418 (**Figure 4A**), indicating the simultaneous occurrence of DNA double-strand breaks induced by

419 CRISPR-Cas9 at these two target sites in the single-cell stage. Many of the other knock-out  
420 mutants showed small indels at the target sites. For example, at target site 2 a 13-bp insertion on  
421 allele 1 and a 2-bp insertion and a 3-bp substitution on allele 2 were identified in the mutant  
422 KO1, most likely because of NHEJ repair (**Figure 4B**). Across all the mutants the lengths of  
423 insertions ranged between 5 and 29 bp, whereas that of deletions varied from 1 to 16 bp  
424 (**Supplementary Table S4**).

425 We noted that the modifications of two alleles at the same target sites were different in all  
426 mutants (**Supplementary Table S4**). For example, two alleles could have indels of different  
427 sizes, or one allele had an insertion whereas the other allele had a deletion, indicating the DNA  
428 repair outcome was often independent between the two alleles. Intriguingly, although induced  
429 mutations occurred at both target sites, no segmental deletions were generated in most of these  
430 knock-out mutants. This was most likely because the induction of DNA double-strand breaks at  
431 different target sites occurred in a sequential manner rather than simultaneously during cell  
432 division.

433 We identified a few mutants that carried unexpected, large deletions (>50bp) at the  
434 *scarlet* locus (**Figure 4D**). For example, in mutant KO2 allele 2 had a segmental deletion of 237  
435 bp spanning the two target sites, whereas allele 1 had a 1569-bp deletion upstream of the target  
436 site 2 (**Figure 4D**). In the mutants KO6.1.3, KO6.3.3, and KO6.3.4, allele 1 had a 1033-bp,  
437 1035-bp, and 1024-bp deletion upstream of the target site 2, respectively (**Figure 4D**). It seems  
438 allele 1 at target site 2 was more vulnerable to large deletion than allele 2, as no large deletions  
439 were found at allele 2 in any mutants.

440 The presence of both black-eyed and clear-eyed neonates in the asexual broods of the  
441 mosaic individuals led us to hypothesize that the asexually produced neonates of the same

442 mother could be derived from primary oocytes with different or no genetic modifications caused  
443 by CRISPR-Cas9 (i.e., mosaicism in the germline cells). To test this hypothesis, we examined  
444 the genotypes of the clear-eyed neonates from the same or different broods of the same mosaic  
445 mother (KO5 and KO6). Within the same brood, neonates in the first brood of KO5 (KO5.1.1  
446 and KO5.1.2) and the first three broods of KO6 (first brood-KO6.1.1, KO6.1.3, KO6.1.4;  
447 second-KO6.2.1, KO6.2.2; third-KO6.3.2, KO6.3.3, KO6.3.4) all carried different genotypes,  
448 whereas the fifth brood of KO6 (KO6.5.1, KO6.5.2, KO6.5.3) had the same genotype for all  
449 neonates (**Supplementary Table S4**). These observations strongly supported our hypothesis.  
450 Across the multiple broods of KO6, we observed the presence of different knock-out genotypes,  
451 substantiating the notion of mosaicism in germline cells. Also, the same genotype appeared in  
452 different broods of the KO6 individual (KO6.3.2 and KO6.4.1), suggesting these neonates were  
453 likely derived from the same primary oocyte cells or different primary oocytes of the same  
454 genetic modification.

#### 455 *Knock-out genotypes induced by Cas12a*

456 Compared to Cas9-induced mutants, our collection of Cas12a-induced knock-out mutants  
457 showed distinct patterns of genetic modification at the two target sites in *scarlet*. We detected  
458 only deletions at the target sites, with their sizes ranging from 1 to 73 bp (**Supplementary Table**  
459 **S4**). Moreover, in three of the four mutants more than one allele-specific target site remained  
460 unmodified, whereas for Cas9-induced mutants only one (KO1) out of 18 mutants had a single  
461 site unmodified (**Supplementary Table S3, S4**). For detailed mutation sequence alignment, see  
462 Supplementary File 1.

#### 463 *Knock-in genotypes at the scarlet locus*

464 Out of the five mutants from our knock-in experiment at target site 2 (mutation sequence  
465 alignment available in Supplementary File 2), we identified two clear-eyed mutant lines (KI4,  
466 KI6) with complete knock-in of the stop-codon cassette in allele 1 based on our reconstruction of  
467 the haplotypes with short-read data. The allele 2 in both KI4 and KI6 harbored a 7-bp insertion at  
468 the target site (**Figure 5**). However, the identified knock-in events were accompanied by  
469 complex local genomic rearrangements in both mutants. In KI4, the insertion of a 240-bp  
470 segment containing the stop-codon cassette with multiple duplicated copies of homology arms  
471 occurred at the location of a 635-bp deletion covering the majority of the target site, resulting in  
472 a net loss of 395 bp (**Figure 5**). In KI6, two versions of allele 1 with knock-in insertion were  
473 observed. In retrospect, this was most likely due to germline mosaicism and complicated our  
474 reconstruction of the insertion haplotypes. Our short-read genomic data allowed us to completely  
475 reconstruct only one haplotype (KI6-hap1), leaving the other one partially resolved (KI6-hap2).  
476 In KI6-hap1 (**Figure 5**), a 116-bp segment containing a stop-codon cassette and a homology arm  
477 was inserted to replace a 635-bp segment (the same deletion tract observed in KI4). For KI6-  
478 hap2, an insertion > 127bp containing multiple duplicated copies of one homology arm occurred  
479 at the target site, accompanied by the deletion of original sequence of unknown length.

#### 480 *Genome-wide mutation rate in scarlet mutants*

481 To determine whether the *scarlet* mutants showed an elevated level of base-substitution  
482 mutations in comparison to the wildtype and whether any mutations were due to the mistarget  
483 effect of Cas9/Cas12a, we examined the genomic DNA sequences of all *scarlet* mutant lines  
484 derived from their 3<sup>rd</sup>/4<sup>th</sup> generation offspring. Using a stringent germline mutation detection  
485 procedure that was experimentally tested with a false discovery rate < 5% (Snyman et al. 2021),  
486 we identified base substitutions in 7 mutant lines with 1-3 base substitutions in each line,

487 whereas the other 17 mutant lines (including the wildtype) had no base substitutions  
488 (**Supplementary Table S7**). None of the base substitutions occurred within or near the possible  
489 mistarget sites of Cas9/Cas12a (with 1 or 2 mismatches to the target sites). The base substitution  
490 rate was on the order of  $10^{-9}$  per site per generation, on par with the spontaneous mutation rate in  
491 *Daphnia* (Keith et al. 2016; Flynn et al. 2017), indicating no elevation of base substitution rate  
492 caused by gene editing.

493 Similarly, our analysis of structural variations (SVs) did not reveal an elevated number of  
494 large indels and duplications. In 20 out of 28 mutant lines, no SVs were detected. Only one  
495 monoallelic insertion event was detected in one mutant (KI6), whereas six hemizygous deletion  
496 events were identified with lengths ranging from 54 to 23,418 bp (**Supplementary Table S8**) in  
497 five mutants. Notably, a 23418-bp hemizygous deletion occurred in KO9. Moreover, two  
498 duplication events were found (297bp and 1735bp). None of these events occurred in genic  
499 regions except for a deletion event in mutant KO5.1.1 overlapping part of gene3461 (kinesin-  
500 related protein 12 signal transduction). Considering that large-scale hemizygous deletion,  
501 insertion and duplications (Xu et al. 2011; Keith et al. 2016) occurs at high rates in the asexual  
502 reproduction in *Daphnia* (on the order of  $10^{-5}$ /bp/generation), the observed deletion rates  
503 (ranging from  $1.12 \times 10^{-7}$  to  $4.86 \times 10^{-5}$  /bp/generation), insertion rate ( $3.07 \times 10^{-7}$  /bp/generation),  
504 and duplication rates (from  $6.17 \times 10^{-7}$  to  $3.6 \times 10^{-6}$ ) were below or on par with the spontaneous  
505 rates (**Supplementary Table S9**).

#### 506 *Spinning behavior in scarlet mutants*

507 Our daily observations of the wildtype vs *scarlet* mutants (day 1 to day 5 post birth) revealed that  
508 while the wildtype swam up and down with small hops and rarely spun themselves, the spinning  
509 behavior exacerbated as the mutant neonates grew up (**Figure 6A**). The movement of mutant

510 female neonates was a combination of normal movement interspersed by episodes of fast  
511 spinning, with the spins on day 1 averaging 7.5 in one minute increasing to 63.1 in one minute  
512 on day 5. We also observed that some mutants tend to perch at the bottom of the vial on their  
513 abdomen or back after fast spinning, which was rarely observed in the wildtype.

#### 514 *Differential gene expression*

515 We performed RNA-seq analyses with three biological replicates of seven *scarlet* mutants each  
516 and the wildtype, totaling 24 samples. An average of 20.9 million (SD=3.5 million) reads were  
517 sequenced per sample. Approximately 99% of the raw reads passed our quality control and  
518 trimming. On average 78% (SD=4.6%) of the retained reads uniquely mapped to the *D. pulex*  
519 reference genome and were used for downstream analyses (**Table S10**).

520 Our pooled differential expression analysis contrasting all mutants' replicates against the  
521 wildtype revealed 328 significantly upregulated genes and 112 genes downregulated in the  
522 scarlet mutant lines compared to the wildtype (**Supplementary Table S11, Supplementary File**  
523 **3**). The number of upregulated genes was significantly higher than downregulated genes (chi-  
524 square test  $p < 0.0001$ ). Among these genes, the *scarlet* gene was significantly downregulated in  
525 the mutants (**Figure 6B**). GO term enrichment analysis showed that various metabolic and  
526 catabolic processes comprised most of the top-ranked GO terms (**Figure 6C, Supplementary**  
527 **Table S12**), with a notable exception of cyclin-dependent kinase serine/threonine kinase activity,  
528 sulfate transport, DNA replication initiation, and signaling. This indicated that the pleiotropic  
529 effects of scarlet knock-out reached beyond the metabolic processes.

530 Through the KEGG pathway enrichment analysis of differentially expressed genes, we  
531 found that the significantly enriched pathways contained Protein digestion and absorption,  
532 Pancreatic secretion, Influenza A, Lysosome, Neuroactive ligand-receptor interaction, Cell

533 adhesion molecules, and Starch and sucrose metabolism (**Figure 6D, Supplementary Table**  
534 **S12**). Nearly all the significantly enriched pathways consisted of only up-regulated genes, with a  
535 mix of up- and down-regulated genes in Protein digestion and absorption (**Figure 6D**).

536         Considering the altered swimming behavior of *scarlet* mutants and neurotransmitter  
537 deficiency noted in the *scarlet* mutant of *D. magna* (Ismail et al. 2021), we further examined the  
538 KEGG pathways relevant for movement and neurological transmission, which were Neuroactive  
539 Ligand-receptor Interaction and Cell Adhesion Molecules. In Neuroactive Ligand-receptor  
540 Interaction, differentially expressed genes included multiple paralogs of trypsin genes,  
541 neuropeptides capa receptor-like gene, and glutamate receptor ionotropic NMDA1. It should be  
542 noted that NMDA1 is involved in neurodevelopmental disorders with movement abnormalities.  
543 For Cell Adhesion Molecules, eight paralogs of contactin-associated protein-like 2 (CNTNAP2)  
544 were upregulated. CNTNAP2 has been found to be associated with multiple neurological  
545 disorders including Autism (Alarcon et al. 2008) and Pitt-Hopkins syndrome (Peippo and  
546 Ignatius 2011).

547         Furthermore, we identified a few non-enriched KEGG pathways that contain highly  
548 differentially expressed genes. In the GABAergic synapse pathway, gene ABAT was  
549 significantly upregulated almost 4-fold in *scarlet* mutants. ABAT gene is known to be involved  
550 in human disease Encephalopathy with uncontrolled limb movements and exaggerated reflexes  
551 (Louro et al. 2016; Koenig et al. 2017). The abovementioned glutamate receptor ionotropic  
552 NMDA1 was 1.6-fold upregulated in *scarlet* mutants and is also associated with the amyotrophic  
553 lateral sclerosis (ALS) pathway.

554         In the individual analysis of each *scarlet* mutant in comparison to the wildtype, the  
555 number of significantly upregulated genes in mutants ranged from 453 to 1111, whereas that of

556 significantly downregulated genes was between 250 to 711 (**Supplementary Table S11**).  
557 Moreover, we generated the consensus set of differentially expressed genes that were shared by  
558 all mutants (i.e., the same direction of expression change  $> 1.5$  fold), consisting of 26 up-  
559 regulated and 5 down-regulated genes (**Supplementary Table S13**). Many genes on this list  
560 were involved in various metabolism pathways (**Supplementary Table S14**). More importantly,  
561 it corroborated several genes that emerged from the pooled analysis including ABAT,  
562 CNTNAP2, and a few paralogs of trypsin. It also drew our attention to a downregulated gene in  
563 the *scarlet* mutant, gene4054 (SLIT2), which is important for axon regeneration and axon  
564 guidance, two fundamental processes in the nervous systems (Curcio and Bradke 2018). We  
565 noted that another gene, gene3375 (SLIT3), which is involved in axon regeneration and axon  
566 guidance, did not enter the consensus list because in one mutant its fold change did not exceed  
567 1.5. However, SLIT3 appeared to be co-regulated with scarlet in our co-expression analysis (see  
568 below).

#### 569 *Gene modules and co-expression analysis*

570 With our gene expression data, a total of 14 gene co-expression modules were obtained. For each  
571 module, module eigengenes were Spearman rank correlated with the *scarlet* knock-out  
572 phenotype. Among the 14 modules identified, six were significant in their correlations with the  
573 *scarlet* mutant phenotype (**Supplementary Figure S1**). The positively correlated modules  
574 (**Supplementary Figures S2-S6**) were magenta ( $\rho = 0.43$ ,  $p = 0.04$ ), red ( $\rho = 0.76$ ,  $p = 1 \times 10^{-5}$ ),  
575 yellow ( $\rho = 0.52$ ,  $p = 0.009$ ), and salmon ( $\rho = 0.6$ ,  $p = 0.002$ ) modules, while negatively  
576 correlated ones were: purple ( $\rho = -0.58$ ,  $p = 0.003$ ) and grey ( $\rho = -0.48$ ,  $p = 0.02$ ).

577 Out of these modules, the red module contained genes that were the most differentially  
578 expressed between the wild-type and *scarlet* knock-out mutant lines. A network was constructed

579 of the differentially expressed genes in this module to visualize the correlations between them  
580 (**Supplementary Figure S2**). The scarlet gene was most positively co-expressed with gene  
581 CTRL (chymotrypsin-like protease CTRL-1), which functions as a protease and hydrolase,  
582 whereas CPA4 and SLIT3 are the most negatively co-expressed genes with scarlet. CPA4, or  
583 carboxypeptidase A4, functions as a protease that hydrolyzes peptide bonds at the carboxy-  
584 terminal end of a protein or peptide. SLIT3, slit homolog 3 protein, is a developmental protein  
585 which aids in the differentiation and development of the nervous system.

## 586 **Discussion**

587 CRISPR gene editing has been successfully implemented in a growing number of emerging  
588 model eukaryotic organisms (e.g., squid, ant, tick) using various effective delivery methods  
589 (Trible et al. 2017; Xu et al. 2019; Crawford et al. 2020; Sharma et al. 2022). These efforts have  
590 paved the way for future functional genomic studies to examine genotype-phenotype relationship  
591 in unprecedentedly diverse organisms. Among these emerging systems, *Daphnia* has excellent  
592 potential for genomic functional studies, largely thanks to the wealth of knowledge accumulated  
593 from decades of research on their evolution/adaptation, ecology, toxicology, phenotypic  
594 plasticity, and response to environmental factors (Altshuler et al. 2011). Since the development  
595 of first-generation *Daphnia* genomic tools (Colbourne et al. 2011), researchers have identified a  
596 large number of candidate genes responsible for various biological processes, such as adaptation  
597 to freshwater salinization (Wersebe and Weider 2023), heavy metal contamination (Shaw et al.  
598 2007), the origin of obligate parthenogenesis and cyclical parthenogenesis (Xu et al. 2015; Xu et  
599 al. 2022; Huynh et al. 2023; Snyman and Xu 2023), and adaptation to ecologically distinct  
600 habitats (Ye et al. 2023), which are ready to be further interrogated for functional insights.

601 As a major tool for functional studies, although microinjection-based CRISPR-Cas9 gene  
602 editing for *Daphnia pulex* has been established (Hiruta et al. 2018), this study addresses several  
603 technical aspects of the microinjection procedure that have not been fully optimized.  
604 Furthermore, through creating *scarlet* gene knock-out mutants, we evaluate the efficiency of  
605 creating heritable mutations with CRISPR-Cas9/Cas12a, the spectrum of on-target mutations,  
606 and potential off-target mutations. Lastly, as *scarlet* appears to be pleiotropic, likely involved in  
607 the production of histamine and other neurotransmitters (Ismail et al. 2021), we examine the  
608 swimming behavior of *scarlet* mutants and the associated transcriptomic profiles to investigate  
609 the pleiotropic effects of *scarlet* and the underlying genetic causes.

#### 610 *Effectiveness of the microinjection procedure*

611 In this study we have developed a robust and effective procedure for generating knock-out  
612 mutants in *D. pulex*. The microinjection procedures in model organisms such as *Drosophila*  
613 (Ringrose 2009), *Caenorhabditis elegans* (Evans 2006), *Anopheles* mosquitoes (Carballar-  
614 Lejarazú et al. 2021) inspired us to develop optimized fabrication for injection needles with  
615 upgraded glass capillary (i.e., aluminosilicate) and repurpose a flipped small Petri dish as the  
616 injection stage for *Daphnia* embryos. We directly inject RNPs instead of plasmids encoding  
617 Cas9/Cas12 and guide RNAs because RNPs can result in mutations at a much greater efficiency  
618 than injecting plasmids or mRNA encoding Cas enzymes (Kim et al. 2014; Hendel et al. 2015).  
619 Most importantly, based on the literature of the development of asexual *Daphnia* embryos  
620 (Ojima 1958; Zaffagnini and Sabelli 1972; Hiruta et al. 2010), we propose and investigate that  
621 approximately 10 minutes post ovulation (1-2 min ovulation time, 6 min in ice-cold medium, and  
622 2-3 min injection time), while the embryos are still in the single-cell stage, provides an effective  
623 time window for inducing heritable biallelic modifications.

624 The results of our CRISPR-Cas9 knock-out experiments at the *scarlet* locus strongly  
625 supported this idea, with a success rate of 1-15% in generating clear-eyed G<sub>0</sub> individuals (**Table**  
626 **1**). More importantly, all the G<sub>0</sub> individuals from the Cas9 experiments carry heritable biallelic  
627 mutations, as evidenced by the clear-eye phenotype in all their offspring, highlighting the  
628 effectiveness of our microinjection strategy.

629 Consistent with the results of Cas9 knock-out experiments, our microinjection  
630 experiments using the A.s. Cas12a nuclease also efficiently generated heritable biallelic  
631 mutations. This is the first successful implementation of CRISPR-Cas12a in *Daphnia* to the best  
632 of our knowledge. The addition of Cas12a to the *Daphnia* gene editing toolkit significantly  
633 expands the range of editable genomic regions beyond what can be achieved with Cas9 nuclease  
634 alone.

635 However, it is notable that our Cas12a knock-out experiments yielded a large portion of  
636 clear-eyed (5 out of 8) mutants due to somatic mutations (i.e., no clear-eyed asexual progenies).  
637 We offer a potential explanation for the lower rate of introducing heritable mutations compared  
638 to the Cas9 knock-out experiments. The A.s. Cas12a nuclease used in this study is temperature  
639 dependent and has low activity level below 30°C (Moreno-Mateos et al. 2017). As 30°C and  
640 above is outside the normal temperature range of *Daphnia pulex*, in our experiments we kept the  
641 Cas12a-injected embryos at 33°C for only two hours post injection and then transferred them to  
642 25°C. The Cas12a nuclease was likely not fully active in the single-cell stage embryo during the  
643 2-hour incubation at 33°C. Thus, the editing activity most likely took place after the one cell  
644 stage and affected only somatic tissues including the eye. A potential solution to increase the  
645 chance of germline modification is to incubate the injected embryos at the (near) optimal  
646 temperature of Cas12a (e.g., 37°C), the detrimental effects of which to the embryos have to be

647 experimentally determined for *Daphnia*. Moreover, as more temperature tolerant versions of  
648 Cas12a nuclease have become available (e.g., Cas12a Ultra from IDT, which was unavailable at  
649 the time of this study), it will be beneficial for future studies to examine its gene editing  
650 efficiency at *Daphnia*-appropriate or out-of-range temperatures.

### 651 *Mosaicism in the germline cells and implications*

652 One of the most interesting findings of this study is the mosaicism in the germline cells of *scarlet*  
653 G<sub>0</sub> mutants, which informs us of the editing process in the embryos and the inheritance of edited  
654 alleles across generations. In general, genetic mosaicism resulting from CRISPR-Cas gene  
655 editing in human and mouse zygotes has been recognized as a consequence of the prolonged  
656 activity of Cas nucleases beyond the first embryo cleavage event (Davies 2019). Although we  
657 intended to create biallelic modification in the one-cell stage of the *Daphnia* embryos, in some  
658 cases the successful editing only occurred after the one-cell stage, affecting different tissues  
659 through independent editing events and resulting in different Cas-induced mutations.

660 It is evident from both our Cas9 and Cas12 experiments that the germline cells of G<sub>0</sub>  
661 individuals (with mosaic *scarlet* phenotype) were differentially edited, which asexually produced  
662 mixed broods of clear-eyed and black-eyed progenies (**Figure 3, Table S2 and S3**). Even among  
663 the clear-eyed progenies of the same mosaic G<sub>0</sub>s, our genomic analyses unveil that their knock-  
664 out *scarlet* genotypes are different (**Table S4**). These observations also suggest that during the  
665 asexual reproduction cycle of *Daphnia*, oogonia going into one asexual brood are derived from  
666 different primary oocytes, rather than one primary oocyte giving rise to all the oogonia.

667 Genetic mosaicism due to gene editing is generally considered a potential risk for clinical  
668 applications (Davies 2019) and could confound downstream analyses of the mutants. Our

669 genomic sequencing of the knock-in mutants was an example of the confounding effect of  
670 germline mosaicism. Without realizing mosaicism and assuming all asexual progenies of a  
671 female *Daphnia* were genetically identical, we pooled all the progenies of KI mutants to  
672 establish a “clonal” mutant line. The presence of more than 2 alleles at the *scarlet* locus in the  
673 genomic sequences of this “clonal” line strongly indicates the presence of germline mosaicism in  
674 the  $G_0$  individual. Nonetheless, germline mosaicism most likely does not exist in the  $G_1$   
675 individuals as all their offspring ( $G_2$ s) exhibit the same phenotype as the mother. There is also no  
676 reason to believe that Cas nucleases could be present in the  $G_1$ s due to transgenerational passing  
677 down from the  $G_0$ s.

678         Despite its confounding effects, we argue that germline mosaicism due to the prolonged  
679 activities of Cas nucleases can be advantageous for *Daphnia* gene editing experiments. This is  
680 because, even in the absence of editing during the one-cell embryo stage, the prolonged nuclease  
681 activities can increase the chances of generating heritable biallelic alterations in the germline  
682 cells. Furthermore, given the independent editing activities in germline cells, multiple knock-out  
683 and knock-in genotypes could appear in the  $G_1$  offspring, facilitating the production of desirable  
684 mutant genotypes.

685         On the other hand, germline mosaicism necessitates a thoughtful plan for *Daphnia*  
686 mutant screening experiments, especially for those focusing on genes with no readily visible  
687 phenotypes. We suggest that a  $G_0$  mom should be maintained through at least two or three  
688 broods. The first-brood individuals of the same mom can be sacrificed for genotyping at the  
689 target locus to identify the presence/absence of mutant alleles. For the matter of efficiency, the  
690 first brood can be pooled for DNA extraction, PCR amplification of target locus, and a T7  
691 endonuclease assay (Parkinson and Lilley 1997) used to detect induced mutations. If mutant

692 alleles are detected from the first brood of a  $G_0$  individual, this  $G_0$  is either a mosaic or pure  
693 mutant. Then each of their second-brood progenies can be used to establish clonal lines that can  
694 be individually genotyped to identify mutant lines. We caution that even if the  $G_0$  mom carries  
695 germline mutations, the first brood could contain no mutant individuals, thus misleading our  
696 conclusions. To mitigate this, one could expand the first round of genotyping to the first two  
697 broods to increase the chance of detecting mutant alleles.

### 698 *Knock-out genotypes and implications*

699 Despite their error-prone nature, nonhomologous end joining (NHEJ) and microhomology-  
700 mediated end joining (MMEJ) are primary pathways for the repair of DNA double-strand breaks  
701 when homologous repair template is not available (Sfeir and Symington 2015). In our Cas9 and  
702 Cas12a knock-out experiments, two gRNAs targeting the scarlet locus were co-injected.  
703 Therefore, we initially expected to see a homozygous segmental deletion if DNA double-strand  
704 breaks occur simultaneously at the two target locations. In the event of only one of the locations  
705 experienced cleavage, we expected to see small indels at one location.

706         However, the genotypes of our knock-out mutants show more complicated DNA repair  
707 outcomes, revealing some under-appreciated aspects of the gene editing process in *Daphnia*  
708 embryos. In fact, clean segmental deletions between two target sites only occurred in two out of  
709 18 knock-out Cas9 mutants (KO2, KO4, **Table S4**), suggesting that Cas-induced cleavage at the  
710 two target locations occurs rarely at the same time, which could be due to their differential  
711 accessibility to the binding of RNPs associated with local nucleosome occupancy or other  
712 factors.

713           The majority of Cas9 mutants show small indels at both of the target locations. The  
714 absence of segmental deletions spanning the two target sites strongly suggests that the DNA  
715 cleavage at these sites did not occur at the same time, most likely one after another. Consistently,  
716 in our Cas12a mutant KO10, only target site 2 had mutations, whereas site 1 had no mutation,  
717 possibly due to reduced activity of Cas12a in our experiments. Furthermore, the induced  
718 modifications on the two alleles are different, suggesting independent repair events. This is  
719 supported by the genotype of our Cas12 mutants KO7 and KO8, where only one allele of either  
720 target site 1 or target site 2 was modified, clearly pointing to the possibility that the DNA  
721 cleavage on the two alleles do not occur at the same time.

722           Furthermore, we find large deletions (>1000bp) at target site 2 in a few Cas9 mutants.  
723 This is not an uncommon DNA repair outcome for Cas9-induced cleavage and has been  
724 previously reported in *C. elegans*, mouse zygote and cultured cells (Shin et al. 2017; Adikusuma  
725 et al. 2018; Au et al. 2019; Davies 2019). As to the repair mechanism generating these  
726 unintended large deletions, MMEJ DNA repair and polymerase theta-mediated end joining has  
727 been proposed as a candidate mechanism (Owens et al. 2019; Schimmel et al. 2023). Although  
728 these large deletions do not disrupt any other coding regions in our *scarlet* mutants, it is crucial  
729 to consider the potential occurrence of large deletions when designing CRISPR target sites and  
730 genotyping mutants. This type of large deletion is hardly detectable through regular PCR. For  
731 example, the genotype of our KO2 sample was initially identified as a homozygous segmental  
732 deletion based on a regular PCR test. However, its genomic sequencing unveiled a segmental  
733 deletion on only one allele, whereas the other allele harbors a large deletion upstream of target  
734 site 2 that removes one primer landing site for our PCR assay, which results in the PCR  
735 amplification of only one allele with segmental deletion as observed in our initial genotyping.

736 *Knock-in efficiency*

737 Homology-dependent repair (HDR) with CRISPR using a DNA donor template is notoriously  
738 inefficient in generating high-fidelity DNA modification (Riesenberg et al. 2023; Schimmel et al.  
739 2023). This is primarily because HDR is inefficient in comparison to NHEJ and MMEJ, which  
740 results in the activation of latter pathways for the imprecise repair of DNA damages (Riesenberg  
741 et al. 2023). Although in the knock-in experiments we chose ssDNA as the donor template,  
742 which boosts HDR efficiency compared to plasmid-based templates, the results of our knock-in  
743 experiment still show inefficient HDR repair. We did not observe any precise editing as  
744 expected, with most mutants not incorporating the stop codon cassette in the repair template. In  
745 the two mutants (KI4, KI6) where incorporation occurred, the insertion of the stop codon cassette  
746 is accompanied by a large 635-bp deletion and other complex rearrangements at the target site. It  
747 is not clear which DNA repair pathway(s) are responsible for this mutagenic outcome. However,  
748 NHEJ-mediated knock-in (Maresca et al. 2013; Auer et al. 2014) seems capable of producing  
749 this kind of knock-in involving complex local rearrangement as seen in another *Daphnia* species  
750 *D. magna* (Kumagai et al. 2017).

751 Numerous strategies for improving the efficiency of HDR repair have been developed,  
752 including inhibiting key proteins of the NHEJ and MMEJ pathways (Riesenberg et al. 2023;  
753 Schimmel et al. 2023) and keeping a close proximity of the HDR repair template with the Cas  
754 components (Aird et al. 2018; Sharon et al. 2018). We note that the microinjection of small-  
755 molecule chemical inhibitors of NHEJ and MMEJ pathway (Schimmel et al. 2023) with RNP  
756 and HDR template into *Daphnia* embryos is worth further investigation because of its simplicity  
757 in implementation.

758 *Off-target mutations in scarlet mutants*

759 Unintended mutagenesis caused by Cas nucleases at non-target genomic locations undermines  
760 the integrity of gene knock-out mutants. Our analyses of base-substitution and structural  
761 variation (SV) mutations in the *scarlet* mutant lines did not show excessive mutations in  
762 comparison to the wildtype, suggesting minimal risks of off-target mutagenesis of Cas9 and  
763 Cas12a in our experiments. Nonetheless, off-target risks need to be assessed in a case-by-case  
764 manner because multiple factors such as the uniqueness of target sites, nuclease concentrations,  
765 and the Cas nuclease variants used in specific experiments could jointly affect the occurrence of  
766 off-target mutations (Davies 2019). Before engaging in an extensive gene editing experiment, it  
767 is now possible to gain an empirical understanding of the off-target effects and genomic location  
768 of mistargets through *in vivo* or *in vitro* methods that combine the digestion of DNA by RNPs  
769 and high-throughput sequencing (Huang and Huang 2023)

#### 770 *Daphnia as an emerging model for neurodegenerative behavior*

771 Our behavioral assay of *scarlet* mutants shows the progression of spinning moves as individual  
772 daphniids grow up. The *scarlet* mutants in *D. magna* also show a similar progression pattern  
773 (Ismail et al. 2021). Interestingly, the spinning moves can be rescued by supplementing  
774 histamine to mutant neonates of *D. magna*, whereas adults' spins are irreversible, suggesting a  
775 progressive neurodegenerative effect of the *scarlet* knock out mutation (Ismail et al. 2021).  
776 However, the rescuing effect of histamine still needs to be verified in *D. pulex*.

777 The progressive nature of the altered swimming behavior in *scarlet* mutants draws an  
778 interesting parallel with the worsening of symptoms in some human neurodegenerative diseases  
779 such as Amyotrophic Lateral Sclerosis (ALS) (Akcimen et al. 2023). Interestingly, the perturbed  
780 transcriptomes of our *scarlet* mutants offer insights into the potential mechanistic basis of this  
781 behavior. Several genes involved in human neurodegenerative diseases such as NMDA1,

782 CNTNAP2, and ABAT are highly differentially expressed in the behavior-changing *scarlet*  
783 mutants compared to the wildtype.

784         These findings provide insight into the pleiotropic effects of the *scarlet* gene and open  
785 opportunities for further understanding the altered gene expression of critical disease-causing  
786 genes in relation to symptom progression. Nonetheless, our transcriptomic data is restricted to 2-  
787 3-day-old female neonates, leaving much to be explored regarding male's behavioral and  
788 transcriptomic responses. As *Daphnia* is nearly transparent with the nervous system easily  
789 visible in the head region with a modern-day microscope, future studies can use single-cell  
790 RNA-seq or spatial transcriptomics to obtain precise neuron-specific transcriptomic profiles and  
791 can *in vivo* tag and track specific proteins across developmental stages in the context of disease  
792 progression. Moreover, the asexual clonal reproduction of *Daphnia* can provide an endless  
793 supply of experimental replicates of the same genetic background. Therefore, we suggest that the  
794 *Daphnia scarlet* mutants provide a powerful model system for understanding the genetic causes  
795 of neurological defects and associated behavioral aberrations from the perspective of faulty ABC  
796 transporter genes.

## 797 **Acknowledgments**

798 We would like to thank J. Dittmer and P. Wright for their assistance with swimming behavior  
799 experiments. We also thank Michael Pfrender for his comments on an early draft of this  
800 manuscript. This work is supported by NIH grant R35GM133730, NSF CAREER grant MCB-  
801 2042490/2348390, NSF EDGE grant 2220695/2324639 to SX.

## References

- 802  
803  
804 Adikusuma F, Piltz S, Corbett MA, Turvey M, McColl SR, Helbig KJ, Beard MR, Hughes J,  
805 Pomerantz RT, Thomas PQ. 2018. Large deletions induced by Cas9 cleavage. *Nature*  
806 **560**: E8-E9.
- 807 Aird EJ, Lovendahl KN, St Martin A, Harris RS, Gordon WR. 2018. Increasing Cas9-mediated  
808 homology-directed repair efficiency through covalent tethering of DNA repair template.  
809 *Communications Biology* **1**: 54.
- 810 Akcimen F, Lopez ER, Landers JE, Nath A, Chio A, Chia R, Traynor BJ. 2023. Amyotrophic  
811 lateral sclerosis: translating genetic discoveries into therapies. *Nat Rev Genet* **24**: 642-  
812 658.
- 813 Alarcon M, Abrahams BS, Stone JL, Duvall JA, Perederiy JV, Bomar JM, Sebat J, Wigler M,  
814 Martin CL, Ledbetter DH et al. 2008. Linkage, association, and gene-expression analyses  
815 identify CNTNAP2 as an autism-susceptibility gene. *Am J Hum Genet* **82**: 150-159.
- 816 Alexa A, Rahnenfuhrer J. 2019. topGO: Enrichment Analysis for Gene Ontology. *topGO*:  
817 *Enrichment Analysis for Gene Ontology*.
- 818 Altshuler I, Demiri B, Xu S, Constantin A, Yan ND, Cristescu ME. 2011. An integrated multi-  
819 disciplinary approach for studying multiple stressors in freshwater ecosystems: *Daphnia*  
820 as a model organism. *Integr Comp Biol* **51**: 623-633.
- 821 Anaka M, MacDonald CD, Barkova E, Simon K, Rostom R, Godoy RA, Haigh AJ,  
822 Meinertzhagen IA, Lloyd V. 2008. The *white* Gene of *Drosophila melanogaster* Encodes  
823 a Protein with a Role in Courtship Behavior. *J Neurogenet* **22**: 243-276.
- 824 Aryal NK, Wasylshen AR, Lozano G. 2018. CRISPR/Cas9 can mediate high-efficiency off-  
825 target mutations in mice in vivo. *Cell Death & Disease* **9**: 1099.
- 826 Au V, Li-Leger E, Raymant G, Flibotte S, Chen G, Martin K, Fernando L, Doell C, Rosell FI,  
827 Wang S et al. 2019. CRISPR/Cas9 Methodology for the Generation of Knockout  
828 Deletions in *Caenorhabditis elegans*. *G3 (Bethesda)* **9**: 135-144.
- 829 Auer TO, Duroure K, De Cian A, Concordet JP, Del Bene F. 2014. Highly efficient  
830 CRISPR/Cas9-mediated knock-in in zebrafish by homology-independent DNA repair.  
831 *Genome Res* **24**: 142-153.
- 832 Bolger AM, Lohse M, Usadel B. 2014. Trimmomatic: a flexible trimmer for Illumina sequence  
833 data. *Bioinformatics* **30**: 2114-2120.
- 834 Borycz J, Borycz JA, Kubów A, Lloyd V, Meinertzhagen IA. 2008. *Drosophila* ABC transporter  
835 mutants *white*, *brown* and *scarlet* have altered contents and distribution of biogenic  
836 amines in the brain.. *J Exp Biol* **211**: 3454-3466.
- 837 Bruce HS, Patel NH. 2022. The carapace and other novel structures evolved via the cryptic  
838 persistence of serial homologs. *Curr Biol* **32**: 3792-3799.
- 839 Carballar-Lejarazú R, Tushar T, Pham TB, James AA. 2021. Microinjection method for  
840 *Anopheles gambiae* embryos. *JoVE (Journal of Visualized Experiments)*: e62591.
- 841 Chen X, Schulz-Trieglaff O, Shaw R, Barnes B, Schlesinger F, Kallberg M, Cox AJ, Kruglyak S,  
842 Saunders CT. 2016. Manta: rapid detection of structural variants and indels for germline  
843 and cancer sequencing applications. *Bioinformatics* **32**: 1220-1222.
- 844 Colbourne JK, Hebert PDN. 1996. The systematics of North American *Daphnia* (Crustacea:  
845 Anomopoda): A molecular phylogenetic approach. *Philos Trans R Soc Lond, B, Biol Sci*  
846 **351**: 349-360.

- 847 Colbourne JK, Pfrender ME, Gilbert D, Thomas WK, Tucker A, Oakley TH, Tokishita S, Aerts  
848 A, Arnold GJ, Basu MK et al. 2011. The ecoresponsive genome of *Daphnia pulex*.  
849 *Science* **331**: 555-561.
- 850 Cong L, Ran FA, Cox D, Lin SL, Barretto R, Habib N, Hsu PD, Wu XB, Jiang WY, Marraffini  
851 LA et al. 2013. Multiplex Genome Engineering Using CRISPR/Cas Systems. *Science*  
852 **339**: 819-823.
- 853 Crawford K, Diaz Quiroz JF, Koenig KM, Ahuja N, Albertin CB, Rosenthal JJC. 2020. Highly  
854 Efficient Knockout of a Squid Pigmentation Gene. *Curr Biol* **30**: 3484-3490 e3484.
- 855 Curcio M, Bradke F. 2018. Axon Regeneration in the Central Nervous System: Facing the  
856 Challenges from the Inside. *Annu Rev Cell Dev Biol* **34**: 495-521.
- 857 Danecek P, Bonfield JK, Liddle J, Marshall J, Ohan V, Pollard MO, Whitwham A, Keane T,  
858 McCarthy SA, Davies RM et al. 2021. Twelve years of SAMtools and BCFtools.  
859 *Gigascience* **10**: giab008.
- 860 Davies B. 2019. The technical risks of human gene editing. *Hum Reprod* **34**: 2104-2111.
- 861 Dobin A, Davis CA, Schlesinger F, Drenkow J, Zaleski C, Jha S, Batut P, Chaisson M, Gingeras  
862 TR. 2013. STAR: ultrafast universal RNA-seq aligner. *Bioinformatics* **29**: 15-21.
- 863 Ebert D. 2022. *Daphnia* as a versatile model system in ecology and evolution. *Evodevo* **13**: 16.
- 864 Evans JM, Day JP, Cabrero P, Dow JAT, Davies SA. 2008. A new role for a classical gene:  
865 *white* transports cyclic GMP. *J Exp Biol* **211**: 890-899.
- 866 Evans T. 2006. Transformation and microinjection. In *Transformation and microinjection*, doi:  
867 doi/10.1895/wormbook.1.108.1. The *C. elegans* Research Community.
- 868 Ewart GD, Cannell D, Cox GB, Howells AJ. 1994. Mutational analysis of the traffic ATPase  
869 (ABC) transporters involved in uptake of eye pigment precursors in *Drosophila*  
870 *melanogaster*. Implications for structure-function relationships. *J Biol Chem* **269**: 10370-  
871 10377.
- 872 Flynn JM, Chain FJJ, Schoen DJ, Cristescu ME. 2017. Spontaneous mutation accumulation in  
873 *Daphnia pulex* in selection-free vs. competitive environments. *Mol Biol Evol* **34**: 160-  
874 173.
- 875 Fu YF, Foden JA, Khayter C, Maeder ML, Reyon D, Joung JK, Sander JD. 2013. High-  
876 frequency off-target mutagenesis induced by CRISPR-Cas nucleases in human cells. *Nat*  
877 *Biotechnol* **31**: 822-826.
- 878 Harris KDM, Bartlett NJ, Lloyd VK. 2012. *Daphnia* as an Emerging Epigenetic Model  
879 Organism. *Genetics Research International* **2012**: 147892.
- 880 Hefferin ML, Tomkinson AE. 2005. Mechanism of DNA double-strand break repair by non-  
881 homologous end joining. *DNA Repair* **4**: 639-648.
- 882 Hendel A, Bak RO, Clark JT, Kennedy AB, Ryan DE, Roy S, Steinfeld I, Lunstad BD, Kaiser  
883 RJ, Wilkens AB et al. 2015. Chemically modified guide RNAs enhance CRISPR-Cas  
884 genome editing in human primary cells. *Nat Biotechnol* **33**: 985-989.
- 885 Hiruta C, Kakui K, Tollefsen KE, Iguchi T. 2018. Targeted gene disruption by use of  
886 CRISPR/Cas9 ribonucleoprotein complexes in the water flea *Daphnia pulex*. *Genes Cells*  
887 **23**: 494-502.
- 888 Hiruta C, Nishida C, Tochinali S. 2010. Abortive meiosis in the oogenesis of parthenogenetic  
889 *Daphnia pulex*. *Chromosome Res* **18**: 833-840.
- 890 Hiruta C, Toyota K, Miyakawa H, Ogino Y, Miyagawa S, Tatarazako N, Shaw JR, Iguchi T.  
891 2013. Development of a microinjection system for RNA interference in the water flea  
892 *Daphnia pulex*. *BMC Biotechnol* **13**: 96.

- 893 Höijer I, Emmanouilidou A, Östlund R, van Schendel R, Bozorgpana S, Tijsterman M, Feuk L,  
894 Gyllensten U, den Hoed M, Ameer A. 2022. CRISPR-Cas9 induces large structural  
895 variants at on-target and off-target sites in vivo that segregate across generations. *Nat*  
896 *Commun* **13**: 627.
- 897 Huang S, Huang X. 2023. A massively parallel approach for assessing CRISPR off-targets in  
898 vitro. *Cell Rep Methods* **3**: 100561.
- 899 Huynh TV, Hall AS, Xu S. 2023. The Transcriptomic Signature of Cyclical Parthenogenesis.  
900 *Genome Biol Evol* **15**.
- 901 Ismail NIB, Kato Y, Matsuura T, Gómez-Canela C, Barata C, Watanabe H. 2021. Reduction of  
902 histamine and enhanced spinning behavior of *Daphnia magna* caused by *scarlet* mutant.  
903 *Genesis* **59**.
- 904 Ismail NIB, Kato Y, Matsuura T, Watanabe H. 2018. Generation of white-eyed *Daphnia magna*  
905 mutants lacking scarlet function. *PLoS One* **13**: e0205609.
- 906 Jinek M, Chylinski K, Fonfara I, Hauer M, Doudna JA, Charpentier E. 2012. A Programmable  
907 Dual-RNA-Guided DNA Endonuclease in Adaptive Bacterial Immunity. *Science* **337**:  
908 816-821.
- 909 Kato Y, Matsuura T, Watanabe H. 2012. Genomic Integration and Germline Transmission of  
910 Plasmid Injected into Crustacean *Daphnia magna* Eggs. *Plos One* **7**.
- 911 Kato Y, Perez CAG, Ishak NSM, Nong QD, Sudo Y, Matsuura T, Wada T, Watanabe H. 2018.  
912 A 5' UTR-Overlapping LncRNA Activates the Male-Determining Gene *doublesex1* in  
913 the Crustacean *Daphnia magna*. *Curr Biol* **28**: 1811-1817.
- 914 Kato Y, Shiga Y, Kobayashi K, Tokishita S, Yamagata H, Iguchi T, Watanabe H. 2011.  
915 Development of an RNA interference method in the cladoceran crustacean *Daphnia*  
916 *magna*. *Dev Genes Evol* **220**: 337-345.
- 917 Keith N, Tucker AE, Jackson CE, Sung W, Lucas Lledo JI, Schrider DR, Schaack S, Dudycha  
918 JL, Ackerman M, Younge AJ et al. 2016. High mutational rates of large-scale duplication  
919 and deletion in *Daphnia pulex*. *Genome Res* **26**: 60-69.
- 920 Kim S, Kim D, Cho SW, Kim J, Kim JS. 2014. Highly efficient RNA-guided genome editing in  
921 human cells via delivery of purified Cas9 ribonucleoproteins. *Genome Res* **24**: 1012-  
922 1019.
- 923 Koenig MK, Hodgeman R, Riviello JJ, Chung W, Bain J, Chiriboga CA, Ichikawa K, Osaka H,  
924 Tsuji M, Gibson KM et al. 2017. Phenotype of GABA-transaminase deficiency.  
925 *Neurology* **88**: 1919-1924.
- 926 Kumagai H, Nakanishi T, Matsuura T, Kato Y, Watanabe H. 2017. CRISPR/Cas-mediated  
927 knock-in via non-homologous end-joining in the crustacean *Daphnia magna*. *Plos One*  
928 **12**: e0186112.
- 929 Langfelder P, Horvath S. 2008. WGCNA: an R package for weighted correlation network  
930 analysis. *BMC Bioinformatics* **9**: 559.
- 931 Li H, Durbin R. 2010. Fast and accurate long-read alignment with Burrows-Wheeler transform.  
932 *Bioinformatics* **26**: 589-595.
- 933 Li H, Handsaker B, Wysoker A, Fennell T, Ruan J, Homer N, Marth G, Abecasis G, Durbin R.  
934 2009. The sequence alignment/map format and SAMtools. *Bioinformatics* **25**: 2078-2079.
- 935 Liang F, Han M, Romanienko PJ, Jasin M. 1998. Homology-directed repair is a major double-  
936 strand break repair pathway in mammalian cells. *Proc Natl Acad Sci USA* **95**: 5172-5177.
- 937 Liao Y, Smyth GK, Shi W. 2014. featureCounts: an efficient general purpose program for  
938 assigning sequence reads to genomic features. *Bioinformatics* **30**: 923-930.

- 939 Louro P, Ramos L, Robalo C, Cancelinha C, Dinis A, Veiga R, Pina R, Rebelo O, Pop A, Diogo  
940 L et al. 2016. Phenotyping GABA transaminase deficiency: a case description and  
941 literature review. *J Inherit Metab Dis* **39**: 743-747.
- 942 Love MI, Huber W, Anders S. 2014. Moderated estimation of fold change and dispersion for  
943 RNA-seq data with DESeq2. *Genome Biol* **15**: 550.
- 944 Mahato S, Morita S, Tucker AE, Liang X, Jackowska M, Friedrich M, Shiga Y, Zelhof AC.  
945 2014. Common transcriptional mechanisms for visual photoreceptor cell differentiation  
946 among Pancrustaceans. *PLoS Genet* **10**: e1004484.
- 947 Mali P, Yang LH, Esvelt KM, Aach J, Guell M, DiCarlo JE, Norville JE, Church GM. 2013.  
948 RNA-Guided Human Genome Engineering via Cas9. *Science* **339**: 823-826.
- 949 Maresca M, Lin VG, Guo N, Yang Y. 2013. Obligate ligation-gated recombination (ObLiGaRe):  
950 custom-designed nuclease-mediated targeted integration through nonhomologous end  
951 joining. *Genome Res* **23**: 539-546.
- 952 Miner BE, De Meester L, Pfrender ME, Lampert W, Hairston NG. 2012. Linking genes to  
953 communities and ecosystems: *Daphnia* as an ecogenomic model. *Proc R Soc Biol Sci B*  
954 **279**: 1873-1882.
- 955 Moreno-Mateos MA, Fernandez JP, Rouet R, Vejnar CE, Lane MA, Mis E, Khokha MK,  
956 Doudna JA, Giraldez AJ. 2017. CRISPR-Cpf1 mediates efficient homology-directed  
957 repair and temperature-controlled genome editing. *Nat Commun* **8**: 2024.
- 958 Moriya Y, Itoh M, Okuda S, Yoshizawa AC, Kanehisa M. 2007. KAAS: an automatic genome  
959 annotation and pathway reconstruction server. *Nucleic Acids Res* **35**: W182-185.
- 960 Nakanishi T, Kato Y, Matsuura T, Watanabe H. 2016. TALEN-mediated knock-in via non-  
961 homologous end joining in the crustacean *Daphnia magna*. *Combining Multiple*  
962 *Hypothesis Sci Rep* **6**: 36252.
- 963 Ojima Y. 1958. A cytological study on the development and maturation of the parthenogenetic  
964 and sexual eggs of *Daphnia pulex*. *Kwansei Gakuin Univ Ann Studies* **6**: 123 - 171.
- 965 Owens DDG, Caulder A, Frontera V, Harman JR, Allan AJ, Bucakci A, Greder L, Codner GF,  
966 Hublitz P, McHugh PJ et al. 2019. Microhomologies are prevalent at Cas9-induced larger  
967 deletions. *Nucleic Acids Res* **47**: 7402-7417.
- 968 Parkinson MJ, Lilley DM. 1997. The junction-resolving enzyme T7 endonuclease I: quaternary  
969 structure and interaction with DNA. *J Mol Biol* **270**: 169-178.
- 970 Peippo M, Ignatius J. 2011. Pitt-Hopkins Syndrome. *Pitt-Hopkins Syndrome* **2**: 171-180.
- 971 Rasys AM, Park S, Ball RE, Alcalá AJ, Lauderdale JD, Menke DB. 2019. CRISPR-Cas9 Gene  
972 Editing in Lizards through Microinjection of Unfertilized Oocytes. *Cell Reports* **28**:  
973 2288-2292.e2283.
- 974 Riesenberger S, Kanis P, Macak D, Wollny D, Dusterhoft D, Kowalewski J, Helmbrecht N,  
975 Maricic T, Paabo S. 2023. Efficient high-precision homology-directed repair-dependent  
976 genome editing by HDRobust. *Nat Methods* **20**: 1388-1399.
- 977 Ringrose L. 2009. Transgenesis in *Drosophila melanogaster*. *Methods Mol Biol* **561**: 3-19.
- 978 Rivera AS, Pankey MS, Plachetzki DC, Villacorta C, Syme AE, Serb JM, Omilian AR, Oakley  
979 TH. 2010. Gene duplication and the origins of morphological complexity in  
980 pancrustacean eyes, a genomic approach. *BMC Evol Biol* **10**: 123.
- 981 Rodgers K, McVey M. 2016. Error-Prone Repair of DNA Double-Strand Breaks. *J Cell Physiol*  
982 **231**: 15-24.
- 983 Schimmel J, Munoz-Subirana N, Kool H, van Schendel R, van der Vlies S, Kamp JA, de Vrij  
984 FMS, Kushner SA, Smith GCM, Boulton SJ et al. 2023. Modulating mutational outcomes

- 985 and improving precise gene editing at CRISPR-Cas9-induced breaks by chemical  
986 inhibition of end-joining pathways. *Cell Rep* **42**: 112019.
- 987 Sekelsky J. 2017. DNA Repair in *Drosophila*: Mutagens, Models, and Missing Genes. *Genetics*  
988 **205**: 471-490.
- 989 Sfeir A, Symington LS. 2015. Microhomology-Mediated End Joining: A Back-up Survival  
990 Mechanism or Dedicated Pathway? *Trends Biochem Sci* **40**: 701-714.
- 991 Sharma A, Pham MN, Reyes JB, Chana R, Yim WC, Heu CC, Kim D, Chaverra-Rodriguez D,  
992 Rasgon JL, Harrell RA et al. 2022. Cas9-mediated gene editing in the black-legged tick,  
993 *Ixodes scapularis*, by embryo injection and ReMOT Control. *iScience*:  
994 doi:<https://doi.org/10.1016/j.isci.2022.103781>.
- 995 Sharon E, Chen SA, Khosla NM, Smith JD, Pritchard JK, Fraser HB. 2018. Functional Genetic  
996 Variants Revealed by Massively Parallel Precise Genome Editing. *Cell* **175**: 544-557  
997 e516.
- 998 Shaw JR, Colbourne JK, Davey JC, Glaholt SP, Hampton TH, Chen CY, Folt CL, Hamilton JW.  
999 2007. Gene response profiles for *Daphnia pulex* exposed to the environmental stressor  
1000 cadmium reveals novel crustacean metallothioneins. *BMC Genomics* **8**: 477.
- 1001 Shin HY, Wang C, Lee HK, Yoo KH, Zeng X, Kuhns T, Yang CM, Mohr T, Liu C,  
1002 Hennighausen L. 2017. CRISPR/Cas9 targeting events cause complex deletions and  
1003 insertions at 17 sites in the mouse genome. *Nat Commun* **8**: 15464.
- 1004 Shirai Y, Piulachs M-D, Belles X, Daimon T. 2022. DIPA-CRISPR is a simple and accessible  
1005 method for insect gene editing. *Cell Reports Methods* **2**: 100215.
- 1006 Snyman M, Huynh TV, Smith MT, Xu S. 2021. The genome-wide rate and spectrum of EMS-  
1007 induced heritable mutations in the microcrustacean *Daphnia*: on the prospect of forward  
1008 genetics. *Heredity (Edinb)* **127**: 535-545.
- 1009 Snyman M, Xu S. 2023. Transcriptomics and the origin of obligate parthenogenesis. *Heredity*  
1010 **131**:119-129.
- 1011 Toyota K, Miyagawa S, Ogino Y, Iguchi T. 2016. Microinjection-based RNA interference  
1012 method in the water flea, *Daphnia pulex* and *Daphnia magna*. In *RNA Interference*.  
1013 IntechOpen.
- 1014 Tribble W, Olivos-Cisneros L, McKenzie SK, Saragosti J, Chang NC, Matthews BJ, Oxley PR,  
1015 Kronauer DJC. 2017. orco Mutagenesis Causes Loss of Antennal Lobe Glomeruli and  
1016 Impaired Social Behavior in Ants. *Cell* **170**: 727-735 e710.
- 1017 Wang H, Xu S. 2021. Something old, something new, a DNA preparation procedure for long-  
1018 read genomic sequencing. *Genome* **65**: 53-56.
- 1019 Wersebe MJ, Weider LJ. 2023. Resurrection genomics provides molecular and phenotypic  
1020 evidence of rapid adaptation to salinization in a keystone aquatic species. *Proc Natl Acad*  
1021 *Sci USA* **120**: e2217276120.
- 1022 Xu S, Huynh TV, Snyman M. 2022. The transcriptomic signature of obligate parthenogenesis.  
1023 *Heredity* **128**: 132-138.
- 1024 Xu S, Omilian AR, Cristescu ME. 2011. High rate of large-scale hemizygous deletions in  
1025 asexually propagating *Daphnia*: omplications for the evolution of sex. *Mol Biol Evol* **28**:  
1026 335-342.
- 1027 Xu S, Pham TP, Neupane S. 2020. Delivery methods for CRISPR/Cas9 gene editing in  
1028 crustaceans. *Marine Life Science & Technology* **2**:1-5

- 1029 Xu S, Spitze K, Ackerman MS, Ye Z, Bright L, Keith N, Jackson CE, Shaw JR, Lynch M. 2015.  
1030 Hybridization and the origin of contagious asexuality in *Daphnia pulex*. *Mol Biol Evol*  
1031 **32**: 3215-3225.
- 1032 Ye Z, Pfrender ME, Lynch M. 2023. Evolutionary Genomics of Sister Species Differing in  
1033 Effective Population Sizes and Recombination Rates. *Genome Biol Evol* **15**.
- 1034 Ye Z, Xu S, Spitze K, Asselman J, Jiang X, Ackerman MS, Lopez J, Harker B, Raborn RT,  
1035 Thomas WK et al. 2017. A new reference genome assembly for the microcrustacean  
1036 *Daphnia pulex*. *G3 (Bethesda)* **7**: 1405-1416.
- 1037 Zaffagnini F, Sabelli B. 1972. Karyologic observations on the maturation of the summer and  
1038 winter eggs of *Daphnia pulex* and *Daphnia middendorffiana*. *Chromosoma* **36**: 193-203.
- 1039
- 1040

1041 **Table 1.** Summary of CRISPR-Cas9 knock-out (KO) and knock-in (KI) experiments for the  
 1042 scarlet gene.

| Experiment | No. of injected embryos | No. of                        | No. of                           | No. of                        |
|------------|-------------------------|-------------------------------|----------------------------------|-------------------------------|
|            |                         | hatching embryos (percentage) | clear-eye Phenotype (percentage) | mosaic phenotype (percentage) |
| KO         | 80                      | 28 (35.0%)                    | 1 (3.6%)                         | -                             |
| KO         | 176                     | 45 (25.6%)                    | 7 (15.6%)                        | -                             |
| KO         | 147                     | 67 (45.6%)                    | 1 (1.5%)                         | -                             |
| KO         | 63                      | 24 (38.1%)                    | 1 (4.1%)                         | -                             |
| KO         | 107                     | 35 (32.7%)                    | 2 (5.7%)                         | 1 (2.9%)                      |
| KO         | 245                     | 100 (40.8%)                   | 1 (1.0%)                         | -                             |
| KI         | 140                     | 80 (57.1%)                    | 1 (1.3%)                         | -                             |
| KI         | 200                     | 117 (58.5%)                   | 4 (3.4%)                         | 3 (2.6%)                      |
| KI         | 235                     | 130 (55.3%)                   | 2 (1.5%)                         | -                             |
| KI         | 204                     | 92 (45.1%)                    | 1 (1.1%)                         | -                             |

1056

1057

1058

1059 **Table 2.** Summary of CRISPR-Cas12 experiments for the scarlet gene.

1060

1061

| Experiment | No. of injected embryos | No. of hatching embryos (percentage) | No. of clear-eye Phenotype (percentage) | No. of mosaic phenotype (percentage) |
|------------|-------------------------|--------------------------------------|---|--------------------------------------|
| KO         | 59                      | 28 (47.5%)                           | 0                                       | 2 (7.1%)                             |
| KO         | 75                      | 28 (37.3%)                           | 1 (3.6%)                                | 2 (7.1%)                             |
| KO         | 131                     | 31 (23.7%)                           | 1 (3.2%)                                | -                                    |
| KO         | 93                      | 25 (26.7%)                           | 4 (16%)                                 | -                                    |
| KO         | 57                      | 21 (36.8%)                           | 1 (4.7%)                                | 4 (19.0%)                            |
| KO         | 69                      | 17 (24.6%)                           | 0                                       | 2 (11.8%)                            |

1075

1076

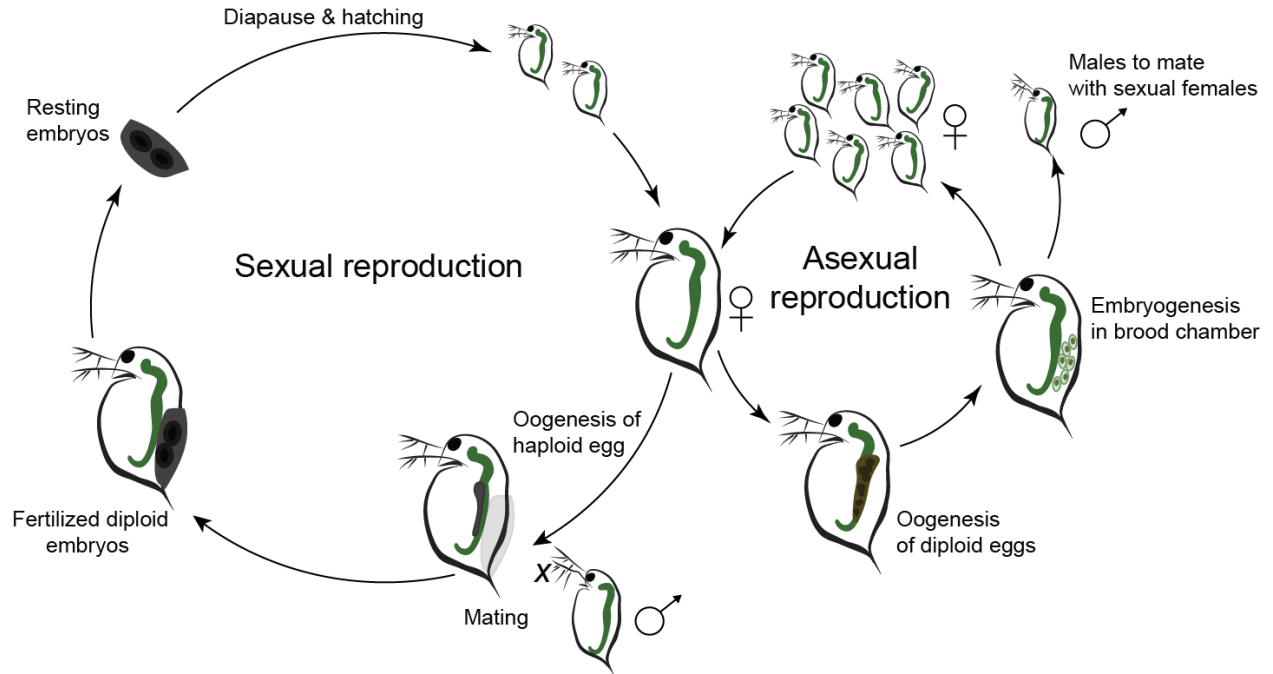
1077

1078

1079 **Figure 1.** The cyclically parthenogenetic life cycle in *Daphnia*.

1080

1081



1082

1083

1084

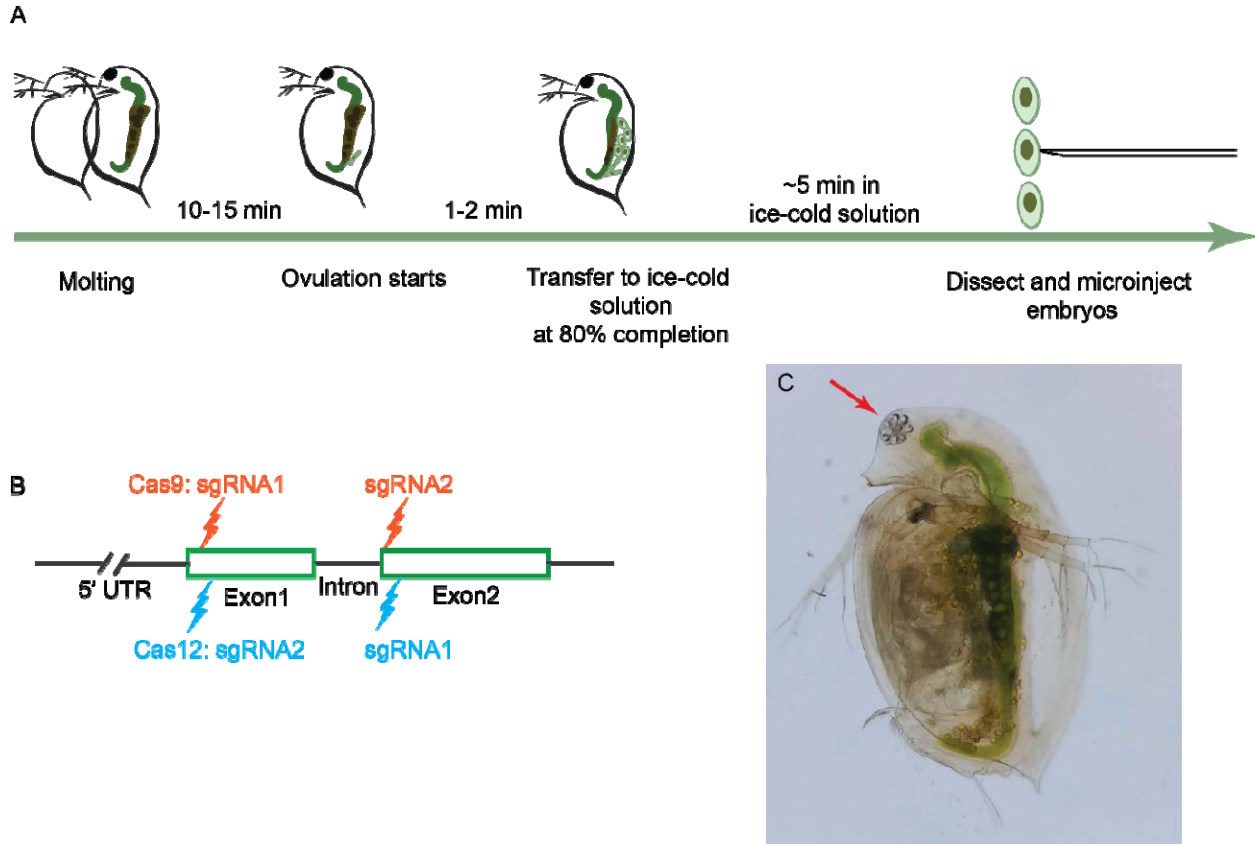
1085

1086

1087

1088 **Figure 2.** (A) The microinjection workflow for CRISPR-Cas9/Cas12 RNP. (B) the schematic  
1089 locations for the guide RNA targets for Cas9 and Cas12 gene editing. (C) The clear-eye  
1090 phenotype (red arrow) caused by the knock-out of scarlet gene.

1091



1092

1093

1094

1095

1096

1097

1098

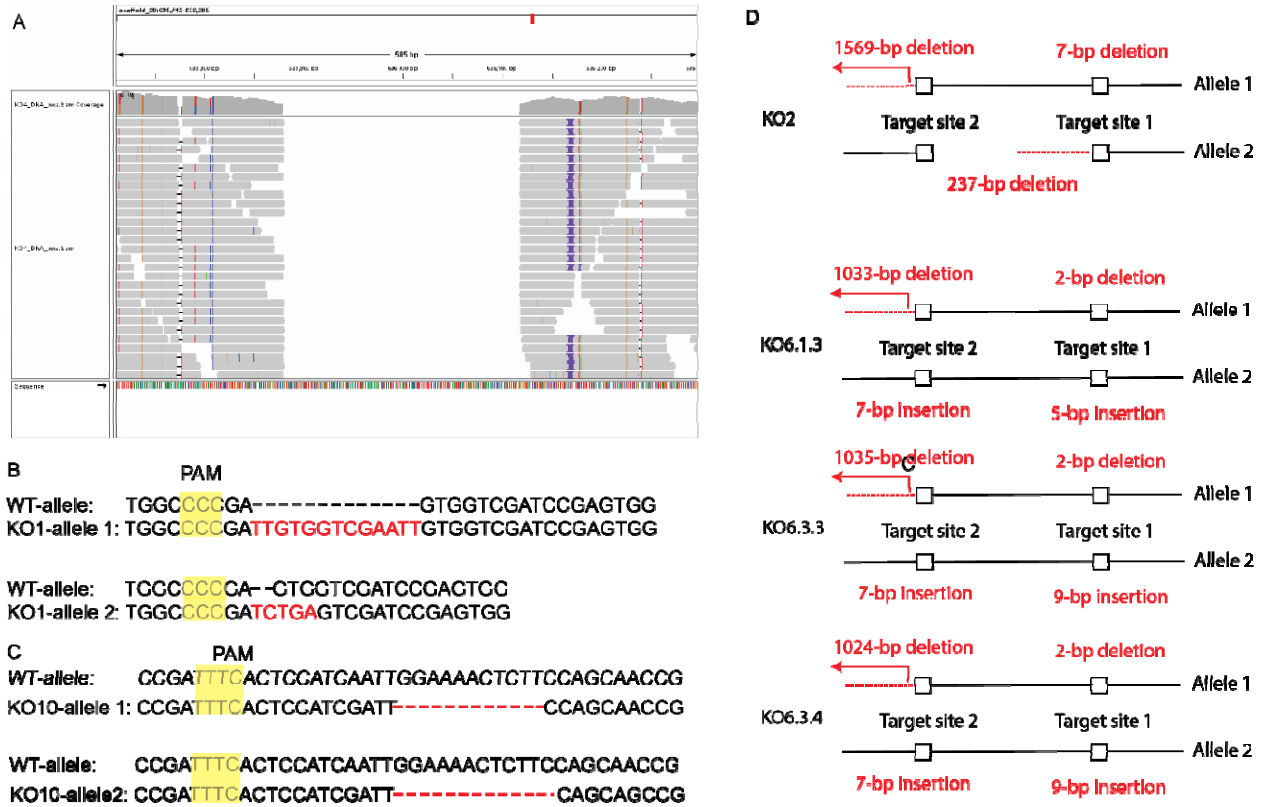
1099

1100

1101



1125 **Figure 4.** Examples of Cas9/Cas12 induced mutations. (A) Short-sequence alignment around the  
 1126 homozygous 234-bp segmental deletion in mutant KO4. Segmental deletion is inferred because  
 1127 of the absence of reads (denoted by grey bars). (B) Cas9-induced allele-specific mutations (red)  
 1128 at target site 2 in mutant KO1. (C) Cas12-induced allele-specific mutations (red) at target site 2  
 1129 in mutant KO10. (D) Mutants with unexpected, on-target hemizygous deletions.



1130

1131

1132

1133

1134

1135

1136

1137

1138

1139

1140

1141



1155 **Figure 6.** (A) The number of spins observed in scarlet mutants KO2 and KO3 in the 8 days post hatching. (B) The transcript  
 1156 abundance of scarlet in wildtype and mutants. (C) Top ranked GO terms from the GO enrichment analysis. Gene ratio is calculated as  
 1157 counts divided by the expected number of genes. (D) The Log2fold distribution of differentially expressed genes in the significantly  
 1158 enriched KEGG pathways. The height of peak represents the number of differentially expressed genes.

1159  
 1160  
 1161  
 1162  
 1163  
 1164  
 1165  
 1166  
 1167  
 1168  
 1169  
 1170  
 1171  
 1172  
 1173  
 1174  
 1175

